NASA CONTRACTOR REPORT

NASA CR-1140

PLATE-GAP MODEL OF A POROUS SOLID AND ITS APPLICATION TO IMPACT BY REDUCED DENSITY PROJECTILES

by J. F. Heyda

Prepared by
GENERAL ELECTRIC COMPANY
King of Prussia, Pa.
for Lewis Research Center

NATIONAL AERONAUTICS AND SPACE ADMINISTRATION • WASHINGTON, D. C. • AUGUST 1968

NASA CR-1140

PLATE-GAP MODEL OF A POROUS SOLID AND ITS APPLICATION TO IMPACT BY REDUCED DENSITY PROJECTILES

By J. F. Heyda

Prepared under Contract No. NAS 3-8512 by
GENERAL ELECTRIC COMPANY
King of Prussia, Pa.

for Lewis Research Center

NATIONAL AERONAUTICS AND SPACE ADMINISTRATION

For sale by the Clearinghouse for Federal Scientific and Technical Information
Springfield, Virginia 22151 – CFSTI price $3.00

FOREWORD

The work described herein was conducted by the Mechanics Section of the Space Sciences Laboratory, General Electric Company, under Contract NAS 3-8512 with the National Aeronautics and Space Administration, Lewis Research Center. Technical direction for the Lewis Research Center was provided by S. Lieblein and I. J. Loeffler of the Airbreathing Engines Division.

ABSTRACT

The sensitivity of the peak axial pressure profiles, obtained using the impact model of an earlier report (NASA CR-609), to a change in the Hugoniot function assumed for the reduced density projectiles is examined briefly. The previous Hugoniot function, based on the Los Alamos equation of state for aluminum, is replaced by one based on the Plate-Gap model of a porous solid due to Thouvenin. A modification of this model is described in detail and its comparison with existing experimental data for six porous materials and the predictions of the theoretically based equation of state due to Wagner and Bjork for aluminum is noted.

Comparison is also made of calculated peak axial pressures obtained using the impact model for the case of normal density aluminum projectiles impacting aluminum with experimental data obtained from corresponding jet projector impact shots conducted by the General Motors Defense Research Laboratory.

PLATE-GAP MODEL OF A POROUS SOLID AND ITS APPLICATION TO IMPACT BY REDUCED DENSITY PROJECTILES

by J. F. Heyda†

General Electric Space Sciences Laboratory

SUMMARY

The plate-gap model of a porous solid, due to Thouvenin, is modified by determining the particle velocity from the momentum-conservation relation and the reflected shock polar of the non-porous solid; the crush-up wave velocity formulation of Thouvenin is retained. This procedure is shown to yield Hugoniot curves for solids, over a wide range of initial porosities, which are in good agreement with available experimental data from Russian and American sources for six materials.

The analytical model for determining peak pressure in an impacted thick target, as given in NASA-CR-609, yields a pressure profile in good agreement with one determined experimentally by the General Motors Defense Research Laboratory for pressures above 150 kb in aluminum. Below this level the analytical model, based on hydrodynamic material behavior, is no longer accurate, the deviation from the experimental profile becoming more pronounced as material strength effects come into play.

Application of the modified plate-gap model Hugoniot data to the calculation of peak axial pressure resulting from impact of aluminum projectiles of varying degrees of porosity with a solid aluminum target resulted in the removal of an apparent anomaly in the target peak pressure profile obtained in a previous study (NASA CR-609).

† Consulting Mathematician, Mechanics Section

INTRODUCTION

In an earlier report (ref. 1) an analytical formulation was presented for evaluating peak pressures in thick targets impacted by hypervelocity projectiles of subnormal bulk densities at normal incidence. It was found that the calculated initial peak pressures at the target surface at impact were greater for the higher density projectiles for equal projectile mass and velocity. Moreover, these pressures were never exceeded by those for the lower density equi-energy projectiles except for the case of the very low density projectiles (0.1 gm/cc and 0.2 gm/cc). For these latter projectiles, the peak pressure at a given distance below the target surface was distinctly higher than that for the projectiles of density 0.44 gm/cc and above, (see Figures 16, 17 of ref. 1).

Since the analytical model used in making the pressure profile calculations was strongly dependent on the form of the Hugoniot function used for the subnormal density projectile material, this anomalous result could only be considered tentative until additional calculations could be made using other, perhaps more accurate, Hugoniots for describing porous material under shock loading. The specific Hugoniot used in reference 1 was obtained from the Los Alamos equation of state† by eliminating the specific internal energy term through use of the energy jump across a shock propagating in the porous material. This Hugoniot, as was pointed out in reference 2 in the case of aluminum, is not sufficiently accurate for the more highly porous initial states. Thus, it is quite appropriate to recalculate the pressure profiles with an alternate description of the Hugoniot states of a porous solid.

This description is furnished by the recently developed Plate-Gap Model for a porous solid due to Thouvenin (refs. 3, 4). Thouvenin replaces a porous solid by a configuration of parallel plates of normal density, the thickness and separation distance of the plates being determined from the known degree of porosity. For this basic configuration Thouvenin derives two fundamental relations: one for the crush-up wave velocity and the other for the particle velocity in the porous material in terms of the shock and particle velocities in the normal density material. In the present report, Thouvenin's relation for the particle velocity behind the crush-up front is replaced by one which combines momentum conservation across the front and the assumption that the shocked porous material unloads along the isentropes of the solid material, the latter being taken as mirror images of the Hugoniot of the solid in the pressure-particle velocity plane. The plate-gap model so modified has been used as the basis for an alternate description of Hugoniot states of an initially porous solid.

† This equation of state is the work of R. K. Osborne and his associates in Group W-4 at the Los Alamos Scientific Laboratory.

The present report contains three parts. The first part presents the Plate-Gap model in detail, including the modification employed for calculating the particle velocity, and detailed calculations of corresponding Hugoniot data for a wide range of porosities. Comparisons are then made with available experimental data from Russian and American sources. Included also are Hugoniot data for porous aluminum given by the Wagner-Bjork equation of state. The second part compares calculated peak axial pressures obtained using the impact model of reference 1 for the case of normal density aluminum projectiles impacting aluminum with unpublished experimental results obtained from corresponding jet projector impact shots at the General Motors Defense Research Laboratory (ref. 5). The concluding section presents the peak axial pressure profiles for the impact cases of reference 1, recalculated using the plate-gap model Hugoniot curves, with a discussion of the differences which arise from use of another Hugoniot representation.

THE PLATE-GAP MODEL

In reference 4 Thouvenin describes a model for the behavior of a porous solid under shock loading which is quite simple. He replaces the solid by an array of parallel plates, each of normal density ρ_o and of thickness $\lambda = \overline{\rho}_o/\rho_o$, where $\overline{\rho}_o$ is the initial density of the porous material; the air gap between any two neighboring plates is taken to be $1-\lambda$. (See Fig. 1). The porous material is thus taken to be periodic in structure, the width of each period being unity and of density $\rho_o\lambda = \overline{\rho}_o$, thereby agreeing with the required initial density. (Symbols are defined in Appendix A).

Consider now a plate impacting the first plate at speed 2u. A shock is driven into it at speed D(u) with corresponding particle velocity u, where D = D(u) is the wave speed in the non-porous material. When the wave reaches the rear free surface of the first plate, the pressurized material of the plate begins to be unloaded by a rarefaction wave moving back toward the front of the plate. The unloaded material then fills in the gap $1-\lambda$ at the free surface velocity $u_{fs} = 2u$. The total time for all this to happen is then (see Figs. 2, 3)

$$\frac{\lambda}{D} + \frac{1-\lambda}{u_{fs}},$$

and this is taken to be the time for the crush-up wave velocity D* in the porous material to cover unit thickness. Hence, we have the first of Thouvenin's relations

$$\frac{1}{D^*} = \frac{\lambda}{D} + \frac{1-\lambda}{2u}, \qquad (1)$$

wherein is used the approximation $u_{fs} \approx 2u$, the validity of which is discussed in some detail in reference 6.

Thouvenin derived a second relation relating u and the crush-up particle velocity u* based on an assumed equilibrium crush-up state. This state is assumed to occur when the shock driven into the unloaded material after its impact with the second plate reaches an asymptotic limiting strength after being attenuated by the unloading waves moving to the left in both first and second plates. Thus, in the time-distance diagram of Figure 3, the shaded areas represent two neighboring plates, the trajectories of the shocks propagating in them at speed D being given by AO and BS. The trajectory of the unloaded material from the rear of the first plate, which fills the gap $1-\lambda$ at speed 2u, is the line segment OB of slope-2u with respect to the t-axis. The crush-up shock wave of speed D* is represented by the line segment OS with slope-D*, the ordinate of the point S being $t_1 = \frac{1}{D^*}$. The

unloading wave in the first plate at time t since its initiation has the trajectory OM of slope $c_1-u_1 = \frac{x}{t}$; c_1 and u_1 being the sound and particle velocities in this plate at this time. Similarly, SM is the unloading wave trajectory up to time t from the rear of the second plate whose slope is $c_2-u_2 = (x+1)/(t-t_1)$. The trajectory of the shock reflected into the unloaded material of the first plate is shown as the curve BM, whose slope at time t is the wave speed $\bar{U} = dx/dt$. Since a shock wave travels supersonically relative to the material in front of it and subsonically relative to the material behind it, the shock will overtake the first unloading wave and will in turn be overtaken by the second. Initially, $\bar{U}$ is constant until the first unloading wave is overtaken, after which $\bar{U}$ is diminished in strength and the shock trajectory becomes curved; this attenuation and subsequent curving is reinforced upon the arrival of the second unloading wave at time t (point M). At this time, Thouvenin determines the trajectory BM approximately, to within second order precision, by taking $\bar{U}$ to be the average of c_1-u_1 and c_2-u_2. This leads to the differential equation for the shock trajectory.

$$\frac{dx}{dt} = \frac{1}{2}\left[\frac{x}{t} + \frac{x+1}{t-t_1}\right], \tag{2}$$

whose solution is readily found to be the hyperbola

$$\frac{x}{\sqrt{t\,|\,t-t_1\,|}} = k - \frac{1}{t_1}\sqrt{\frac{t}{|t-t_1|}}, \tag{3}$$

where k is a constant of integration which is determined by passing the curve through the point B $\left(\lambda-1, \frac{1-\lambda}{2u}\right)$. After some effort we find

$$k = |\,2u + D^*\,|\sqrt{\frac{(1-\lambda)D}{2u\lambda}}. \tag{4}$$

The assumed equilibrium crush-up state is now defined as that state for which $\bar{U}$ reaches its asymptotic value, namely the slope of the appropriate asymptote of (3). At this time the speeds c_1-u_1 and c_2-u_2 will have merged into coincidence with the asymptotic $\bar{U}$ value, so that

$$\bar{U}_{\text{asymp.}} \equiv c^* - u^* = k - \frac{1}{t_1}, \tag{5}$$

where now u^* is the equilibrium state crush-up particle velocity and c^* is the sound speed in the material behind the shock with strength given by (5). Thouvenin adopts the empirical rule,

$$c = A + (2B-1)\,u \quad , \tag{6}$$

relating sound and particle speeds behind a shock propagating in the non-porous plate material, where A and B are empirical constants, and assumes the isentropic unloading path for the shock-loaded porous solid (arc PAB of Figure 2) to be the mirror image of the Hugoniot OP with respect to the vertical PC. With this assumption c* can be obtained by replacing u in (6) by 2u - u*, whence we find

$$c^* - u^* = A + (2B-1)\,2u - 2B\,u^* \quad . \tag{7}$$

Combining (5) and (7) then yields the following result for u*:

$$u^* = \frac{1}{2B}\left[A + 2\,(2B-1)\,u + D^* - k\right], \tag{8}$$

where u is known and D* and k are obtained from (1) and (4), respectively. The constants A, B are the same ones which appear in the classical empirical relation, D = A + Bu, relating shock and particle velocities in a given material, for which an extensive tabulation is given in reference 6.

Equations (3), (4), (5), (8) do not appear in Thouvenin's paper but are derived here on the basis of the procedure which Thouvenin prescribes. Actually, Thouvenin simplified the procedure still more by omitting one of the unloading waves in Figure 3, thereby simplifying the differential equation (2) and obtaining a parabola for the shock trajectory. He does not give the corresponding formula for u*. However, he does plot p* vs u* for porous copper at moderate pressures, where relation (8) agrees with his plot reasonably well. At higher pressures, as might be expected from the type of approximations made, relation (8) is quite inaccurate. For this reason an alternate relation for the computation of u* to replace equation (8) has been developed.

MODIFIED PLATE-GAP MODEL

The experimental evidence presented by Thouvenin (ref. 4) in support of relation (1) for the case of porous copper and, to a lesser extent, porous aluminum and uranium, is most convincing. For this reason relation (1) will be assumed to be valid without amendment. It is proposed, however, to calculate u* by the following procedure. One notes from the physics of the situation and from Figure 2 that u* will lie between u and 2u and that by virtue of symmetry the corresponding pressure p* can be obtained from the shock polar for the non-porous solid, p = F(u), evaluated at 2u-u*. Thus,

$$p^* = F\,(2u-u^*)\,. \tag{9}$$

If now one keeps the Hugoniot relation for conservation of momentum across the crush-up shock front, we shall also have

$$p^* = \bar{\rho}_o\, D^*\, u^*\,. \tag{10}$$

From the equality of (9) and (10), we then have the necessary relation for calculating u*:

$$F\,(2u-u^*) = \bar{\rho}_o\, D^* u^* \tag{11}$$

This is in contrast to Thouvenin's procedure of calculating u* by an independent relation like (8) and then getting p* from (9).

For a given material, then, of porosity λ the modified procedure for calculating shock velocity D*, induced by plate impact at speed 2u, and the pressure p* behind this shock with accompanying particle speed u*, is summarized, respectively, by relations (1), (10) and (11).

Calculated curves of p* and D* vs u*, and of p* vs ρ^*/ρ_o for porosities m ranging from 1 to 6.14 are presented in Figures 4 through 9 for aluminum, copper, lead, iron, nickel and tungsten. The (D*, u*)-plots, for given λ, are based on equations (1), (11) with u regarded as a parameter; the function F(u) for the non-porous solid was available from the Los Alamos formulation (see pp. 13, 14 of ref. 1). Values of D* and u*, when substituted into equation (10), furnish values of p* for the (p*, u*)-plots. The values of ρ^*/ρ_o to be coupled with the p* values are given by the continuity of mass relation across the crush-up front, namely

$$\frac{\rho^*}{\rho_o} = \frac{\lambda D^*}{D^*-u^*}\,. \tag{12}$$

Experimental data for each of the six metals, taken from references 6 through 11, are also plotted. In addition, in the case of aluminum, points (Fig. 4) are plotted from the Hugoniot curves implied by the Wagner-Bjork equation of state (ref. 2).

As is evident, the modified plate-gap model computations show excellent agreement with experiment and, in the case of aluminum, with the Wagner-Bjork points, on the (p*, u*) and (D*, u*) plots. On the plots of pressure versus compression, (p*, ρ^*/ρ_o), the agreement between theory and experiment ismixed: excellent for some of the data points, poor for others. In view of the excellent agreement in the case of the (D*, u*) and (p*, u*)-plots, the reason for this is not altogether clear. Experimentally, it is D* that is measured and the other variables are then calculated from it using the Hugoniot relations. The relative errors in p* and u* are related to the relative error in D* by (see Appendix B)

$$\frac{\Delta u^*}{u^*} = -\frac{1}{2}\frac{\Delta D^*}{D^*}\ , \quad \frac{\Delta p^*}{p^*} = \frac{1}{2}\frac{\Delta D^*}{D^*}\ . \tag{13}$$

Thus, a good measurement of D* yields smaller relative errors for p* and u*. The relative error in the compression, $\sigma^* = \rho^*/\rho_o$, as equation (B.6) shows, depends upon the compression and the porosity:

$$\frac{\Delta \sigma^*}{\sigma^*} = -\frac{3}{2}\,(m\sigma^* - 1)\,\frac{\Delta D^*}{D^*}\ . \tag{14}$$

The factor $\frac{3}{2}(m\sigma^*-1)$ is larger than 1 whenever $\sigma^* > \frac{5/3}{m}$. The latter was true for all but one of the experimental porous data points plotted. This suggests that, in general, relative errors in the compression are larger than corresponding relative errors in the measured shock velocity D*, the amplification increasing with the porosity. The departure of the experimental data points from the modified plate-gap model curves in the pressure-compression plane may be due both to the errors in the pressure and the compression resulting from a given error in the shock velocity and also to the fundamental inadequacy of the model itself. How to separate these effects in evaluating the model is an additional problem for which no answer is now available.

APPLICATION TO IMPACT BY REDUCED DENSITY PROJECTILES

An analytical model for determining peak axial pressure in a thick target impacted at normal incidence by end-on oriented right circular cylindrical projectiles of either normal or subnormal bulk density travelling at hypervelocity was presented in detail in reference 1. This model takes into account the speed and geometry (radius L and length ℓ) of the projectile, its density and that of the target, and the speed of sound in the undisturbed target material. It is based on combining the Hugoniot relations for the thermodynamic state back of the shock advancing into the target with a kinematic relation expressing the axial speed of the shock as a function of its axial position. Empirical constants appearing in the kinematic relation are evaluated from a knowledge of the location of the axial point where the shock is first attenuated by lateral rarefaction waves originating at the projectile periphery at impact and from empirical formulations based on numerical solutions of the equations defining the impact generated flow in the target. The kinematic relation itself is based on a blast wave interpretation for the axial shock speed, expressing the latter as a linear combination of the speeds of planar and cylindrical blast waves.

Experimental data are now available to verify the accuracy of the model (ref. 5). These data of pressure against distance in aluminum targets were obtained by the General Motors Corporation Defense Research Laboratory under contract with the NASA-Lewis Research Center. The experimental data are presented for an impact into an 1100-0 aluminum target at 11.15 km/sec. by a solid aluminum projectile weighing 0.585 gm with a length to diameter ratio (ℓ/2L) of 3.3. In reference 5 peak axial pressure against distance into the target was represented by a straight line on log-log paper. This relation is shown by the solid line in Figure 10.

When the peak axial pressure model of reference 1 is applied to this particular impact case, the profile obtained is the curved dashed line of Figure 10. Above 150 kb this profile is, within experimental error, coincident with the experimental profile of reference 5. Below 150 kb the two profiles diverge since the profile of reference 1 becomes invalid at lower pressures. This is because the profile of reference 1 is based on a purely hydrodynamic model of material behavior. Below 150 kb the aluminum target begins to exhibit behavior markedly different from that of a perfect fluid.

In reference 1, hypervelocity impacts of equi-mass aluminum projectiles of densities 2.702, 0.9, 0.44, 0.2 and 0.1 gm/cc into a thick aluminum target were investigated using the peak pressure model. Two impact velocities were considered, 20 km/sec and 7.6 km/sec. The purpose

was to investigate variation in peak axial pressure propagating into the target as a function of projectile density. It was found that at 20 km/sec, the peak pressure profiles in the target due to impacts of the projectiles of densities 2.702, 0.9 and 0.44 gm/cc were, beyond a short distance into the target, essentially indistinguishable. For the low density projectiles of 0.1 and 0.2 gm/cc, however, the peak pressure profiles generated in the target, beyond a certain distance into the target, lay above the profiles arising from the higher density projectile impacts. The same situation was found to hold for the profiles generated by impacts at 7.6 km/sec. As was pointed out in reference 1, this anomalous result could only be considered tentative in view of the strong dependence in the analytical model on the form of the Hugoniot function used for the subnormal density projectile material. The situation will now be re-examined using an alternate Hugoniot representation.

For the peak axial pressure model of reference 1, the Hugoniot values of pressure, density, shock and particle velocities in the target at impact are required as inputs. In Figures 16 and 17 of reference 1, the Hugoniot values were obtained based on the Los Alamos equation of state for aluminum. The present calculations use Hugoniot values based on the Modified Plate-Gap Model.

Figures 11 and 12 show the plots of recalculated peak axial pressure versus shock penetration distance into a solid aluminum target arising from impacts at speeds of 20 and 7.6 km/sec, respectively, of four aluminum projectiles, all of the same mass, but of densities 2.702, 0.90, 0.44, and 0.20 gm/cm^3. The projectiles are taken to be right circular cylinders with length ℓ and radius L equal to 1/2 ℓ and are assumed to impact end-on at normal incidence. The values of L associated with these densities are, respectively, 0.2619, 0.3778, 0.4797, and 0.6238 cm.

Figure 11 is noticeably different than Figure 16 of reference 1. Whereas, formerly, the pressure profiles for reduced density projectiles of 0.44 gm/cm^3 and higher showed coalescence, indicating, at least for this range of densities, no pronounced density effect, the profiles corresponding to the reduced density projectiles now lie distinctly below that for the projectile of normal density. In addition, the formerly anomalous result in which the profile corresponding to the projectile of density 0.20 gm/cm^3 lay above the normal density profile is no longer present.

If one interprets cratering in a thick target in terms of the impact-generated pressure pulse propagating therein, the anomaly of reference 1 suggests, contrary to physical intuition, that very low density projectiles have greater penetration power into thick targets than higher density projectiles of the same mass and impact velocity. The present result, for 20 km/sec impacts, implies then reduced crater depths in thick targets impacted by highly porous projectiles.

An apparent anomaly is still present in Figure 12 for the 7.6 km/sec impact. The pressures in Figure 12 for the 0.20 gm/cm^3 case all lie below 100 kb, and in this low range of pressures the peak axial pressure model of reference 1 no longer applies since it was based on a purely hydrodynamic model of material behavior. Credence for this statement is supplied by Figure 10, where an experimental pressure profile for an impact into aluminum of a solid aluminum projectile of mass 0.585 gm at 11.15 km/sec is compared with that predicted by the model of reference 1. The two profiles coincide from 1 Mb down to 150 kb, after which there is rapid divergence. Thus, it is argued that for the 7.6 km/sec impact of a projectile of density 0.20 gm/cm^3, the location of its pressure profile above that of the normal density profile is meaningless since at the low pressures involved neither of the profiles is valid.

The conclusion which appears warranted from these results is that the anomalous inversion of the profiles corresponding to projectile densities of 0.20 and 2.702 gm/cm^3 for equi-energy impacts at 20 km/sec arises from the use of inaccurate Hugoniot data for the reduced density projectile and that the same situation at 7.6 km/sec is invalid owing to the inapplicability of the analytical model at the low pressures encountered. As demonstrated by the curves in Figures 4 thru 9 with relation to the available experimental data, the modified plate-gap model can be relied upon to furnish accurate Hugoniot data for impact calculations.

CONCLUSIONS

1. The plate-gap model of a porous solid, as modified in this report, can be used to generate Hugoniot data for solids over a wide range of initial porosities. This is confirmed by good agreement with available experimental data from both Russian and American sources.

2. It is shown that the analytical model for determining peak axial pressure in an impacted thick target, as developed in NASA CR-609, yields a pressure profile in good agreement with one determined experimentally by the General Motors Defense Research Laboratory for pressures above 150 kb in aluminum. Below this level the analytical model, based on hydrodynamic material behavior is inapplicable.

3. When the modified plate-gap model Hugoniot values are applied to the calculation of peak axial pressures resulting from impact of aluminum projectiles of varying degrees of porosity with a solid aluminum target, previously obtained results of an anomalous nature (NASA CR-609) either disappear or can be shown to be inapplicable. At a given axial position in the target, reduced projectile density results in reduced pressure in all applicable cases.

APPENDIX A

SYMBOLS

A	constant in relation $D = A + Bu$
B	constant in relation $D = A + Bu$
c	speed of sound
D	shock velocity
F	shock polar function
L	radius of cylindrical projectile
ℓ	length of cylindrical projectile
m	porosity ratio, $\rho_o/\overline{\rho}_o$
p	pressure
t	time
u	particle velocity
x	abscissa
λ	$1/m$
ρ	density behind shock
ρ_o	undisturbed target density
$\overline{\rho}_o$	reduced density of porous projectile

Subscripts

fs	free surface value

Superscript

*	indicates value of given quantity for porous material

APPDENDIX B

DETERMINATION OF RELATIVE ERROR RELATIONS

For a planar, steady-state shock of strength p* propagating in a porous material, the work performed per unit area per unit time is constant, that is

$$p^* u^* = \text{const.}$$

Since $p^* = \lambda \rho_o D^* u^*$, we have

$$D^* u^{*2} = \text{const},$$

whence

$$\frac{\Delta u^*}{u^*} = -\frac{1}{2} \frac{\Delta D^*}{D^*} . \tag{B.1}$$

From the conservation of mass across the crush-up front, denoting ρ^*/ρ_o by σ^*, we have

$$\frac{u^*}{D^*} = \frac{m\sigma^* - 1}{m\sigma^*} , \tag{B.2}$$

whence

$$\frac{\Delta u^*}{u^*} = \frac{\Delta D^*}{D^*} + \frac{1}{m\sigma^* - 1} \frac{\Delta \sigma^*}{\sigma^*} . \tag{B.3}$$

From $p^* = \lambda \rho_o D^* u^*$, we have

$$\frac{\Delta p^*}{p^*} = \frac{\Delta D^*}{D^*} + \frac{\Delta u^*}{u^*} . \tag{B.4}$$

Combining (B.1) and (B.4) then yields

$$\frac{\Delta p^*}{p^*} = \frac{1}{2} \frac{\Delta D^*}{D^*} . \tag{B.5}$$

Similarly, combining (B.1) and (B.3) yields

$$\frac{\Delta \sigma^*}{\sigma^*} = -\frac{3}{2} (m\sigma^* - 1) \frac{\Delta D^*}{D^*} . \tag{B.6}$$

REFERENCES

1. Heyda, J. F., and Riney, T. D.: Peak Pressures in Thick Targets Generated by Reduced Density Projectiles, NASA CR-609, 1966.

2. Wagner, M. H. and Bjork, R. L.: Impact of a Porous Aluminum Projectile on Aluminum at 20 and 72 km/sec, Seventh Hypervelocity Impact Symposium Proceedings, Vol. III, February 1965, pp. 1-54.

3. Thouvenin, J.: Action d'une Onde de Choc sur un Solide Poreaux, Comptes Rendus, 258 (April 1964), 3461-3464.

4. Thouvenin, J.: Action d'une Onde de Choc sur un Solide Poreaux, Fourth Symposium on Detonation, U. S. Naval Ordnance Laboratory, Silver Spring, Maryland, Vol. B, October 1965, pp. 146-155.

5. Wenzel, A.B. and Clough, N.: "Target Pressure and Damage Data from Impacts by Explosively-Propelled Projectiles", NASA TM X-1597, 1968.

6. Rice, M.H., McQueen, R.G., and Walsh, J.M.: Compression of Solids by Strong Shock Waves, Solid State Physics, Vol. 6, pp. 29-30, Academic Press, 1958.

7. Kormer, S.B., et al: Dynamic Compression of Porous Metals, Soviet Physics JETP, Vol. 15, No. 3, September 1962, pp. 477-488.

8. Krupnikov, K.K., et al: Shock Compression of Porous Tungsten, Soviet Physics JETP, Vol. 15, No. 3, September 1962, pp 470-476.

9. Anderson, G.D., Doran, G.G., Fahrenbruch, A.L.: Equation of State of Solids: Aluminum and Teflon, Air Force Weapons Laboratory, Technical Report No. AFWL-TR-65-147, December 1965.

10. Alt'shuler, L.V. et al., "Dynamic Compressibility and Equation of State of Iron under High Pressure", Soviet Physics JETP, 34 (7), No. 4, October 1958, pp. 606-614.

11. Marsh, S.P. and McQueen, R.G., "Equation of State for Nineteen Metallic Elements from Shock-wave Measurements to Two Megabars", J. Appl. Phys. 31, No. 7 (July 1960) 1253-1269.

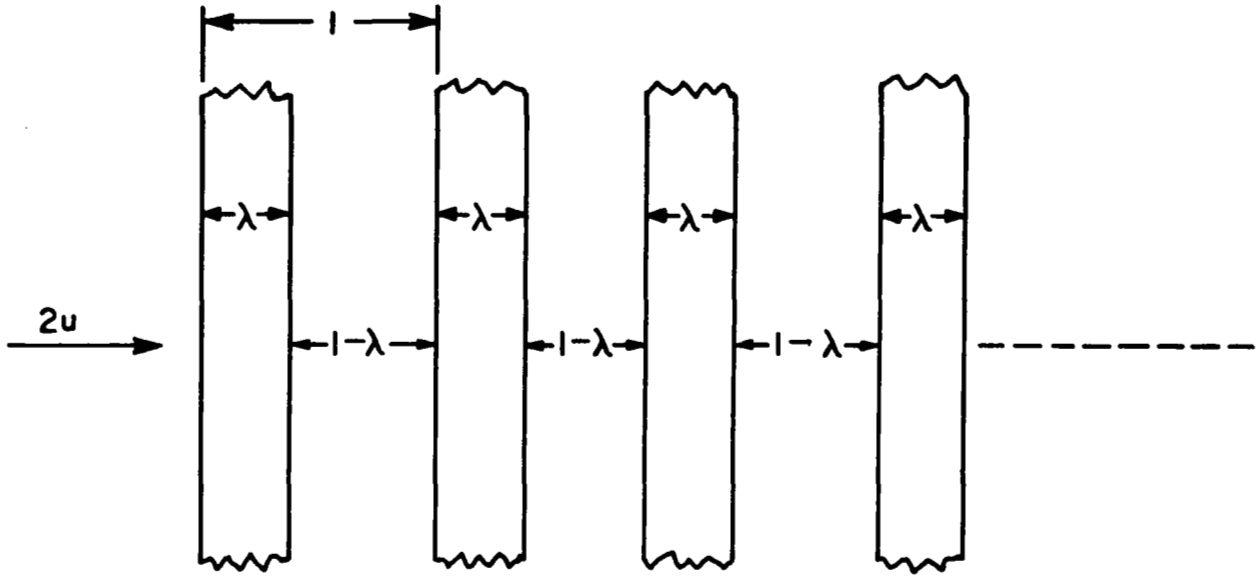

Figure 1. Plate-Gap Model of a Porous Solid

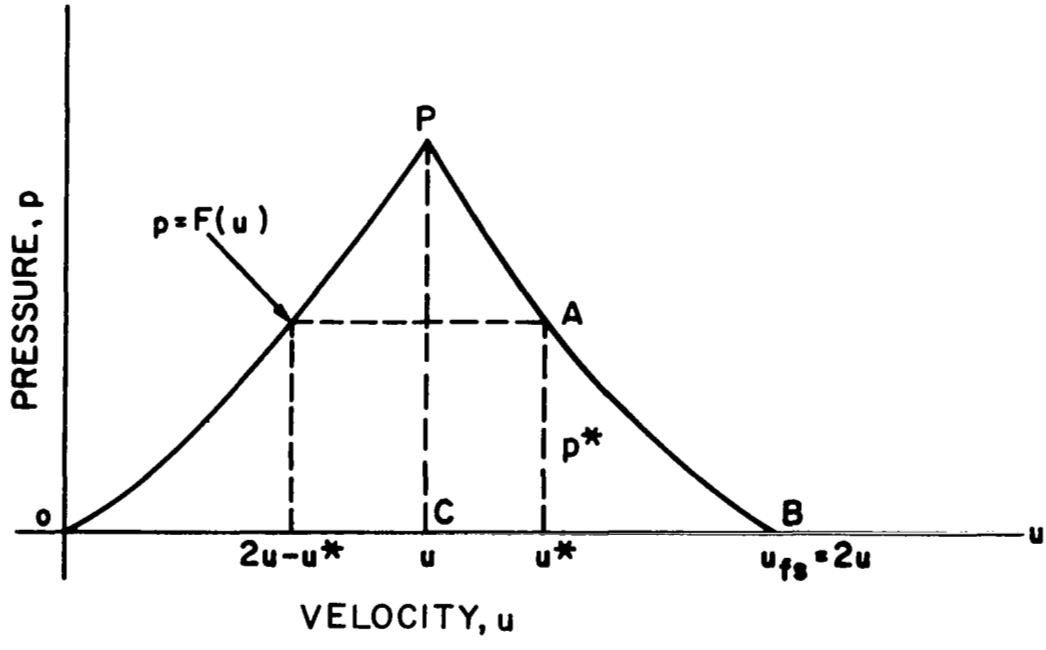

Figure 2. Loading and Unloading Paths for a Porous Solid

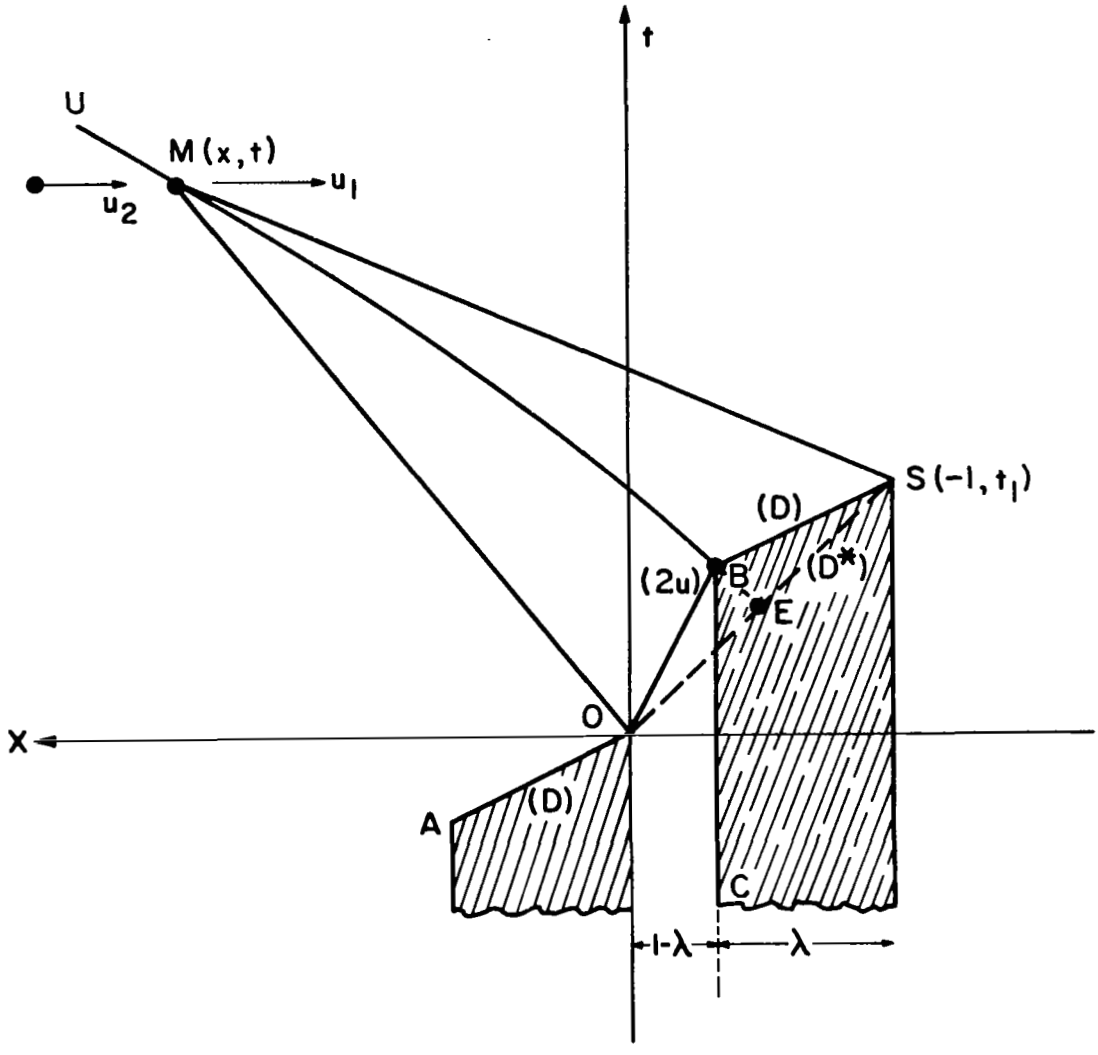

Figure 3. Diagram for Determining an Equilibrium Crush-Up State

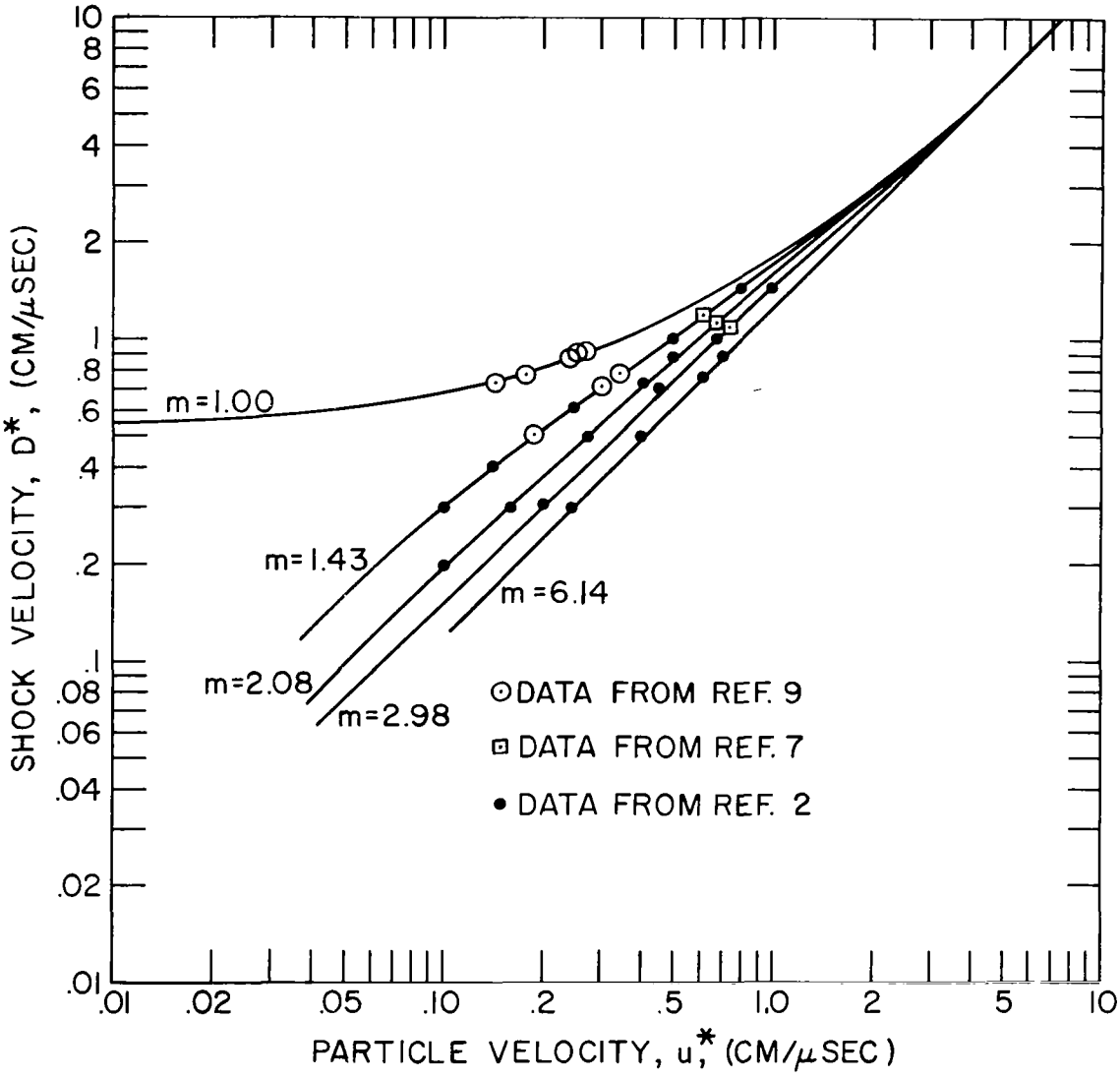

Figure 4. Hugoniots for Porous Aluminum - Modified Plate-Gap Model
(a) Shock Velocity vs Particle Velocity

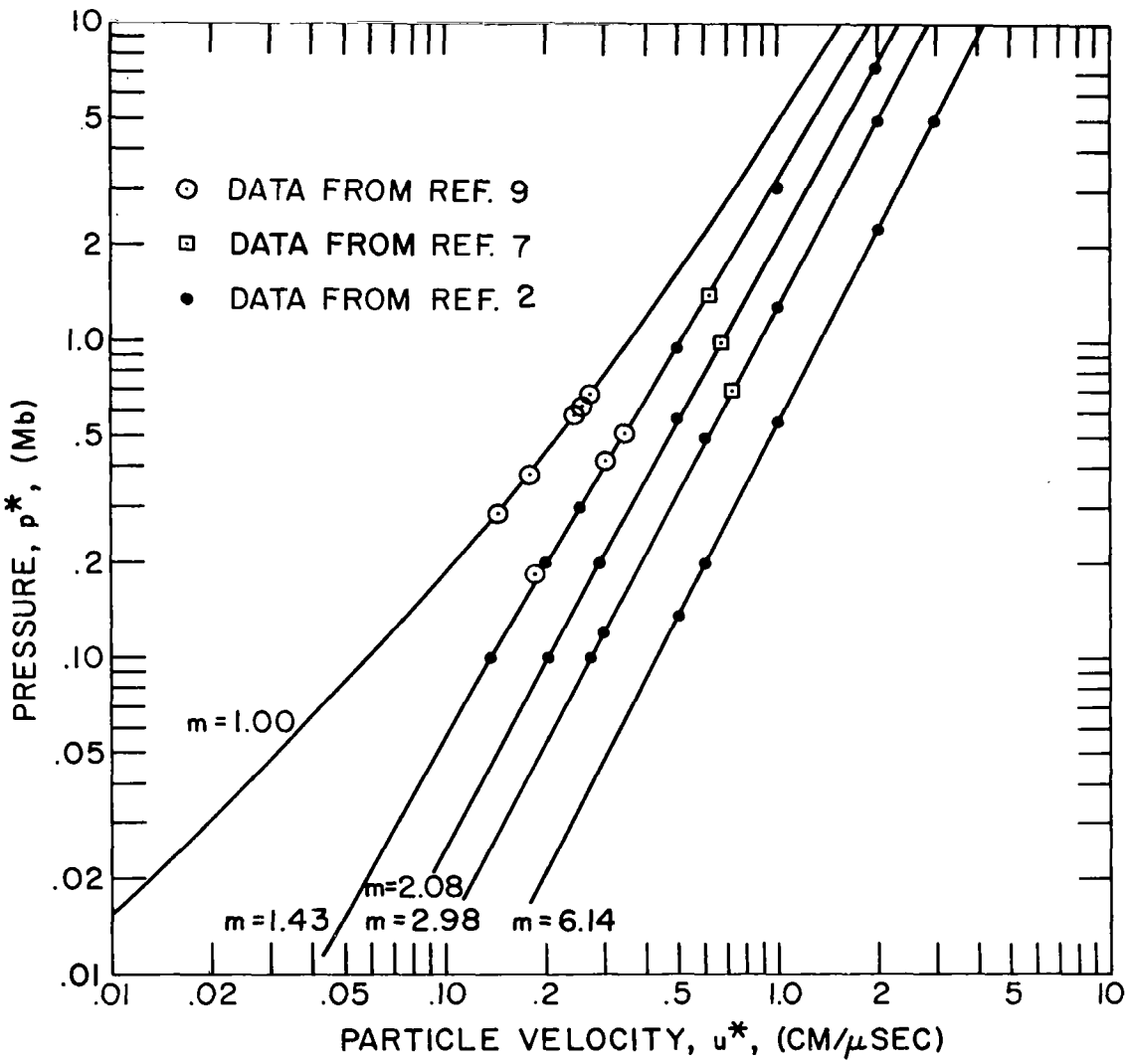

Figure 4. Hugoniots for Porous Aluminum - Modified Plate-Gap Model
(b) Pressure vs Particle Velocity

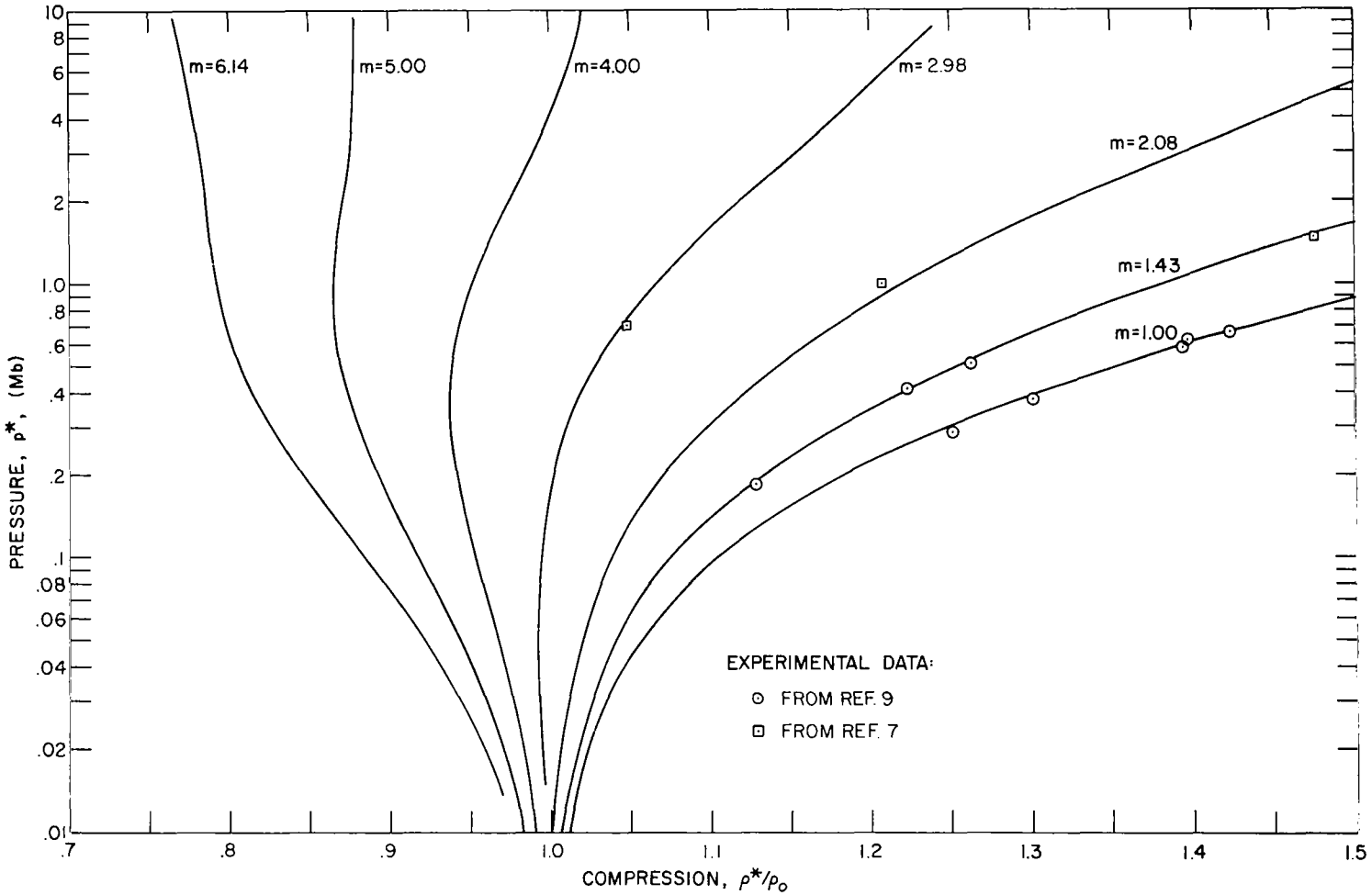

Figure 4. Hugoniots for Porous Aluminum, Modified Plate-Gap Model
(c) Pressure vs Compression

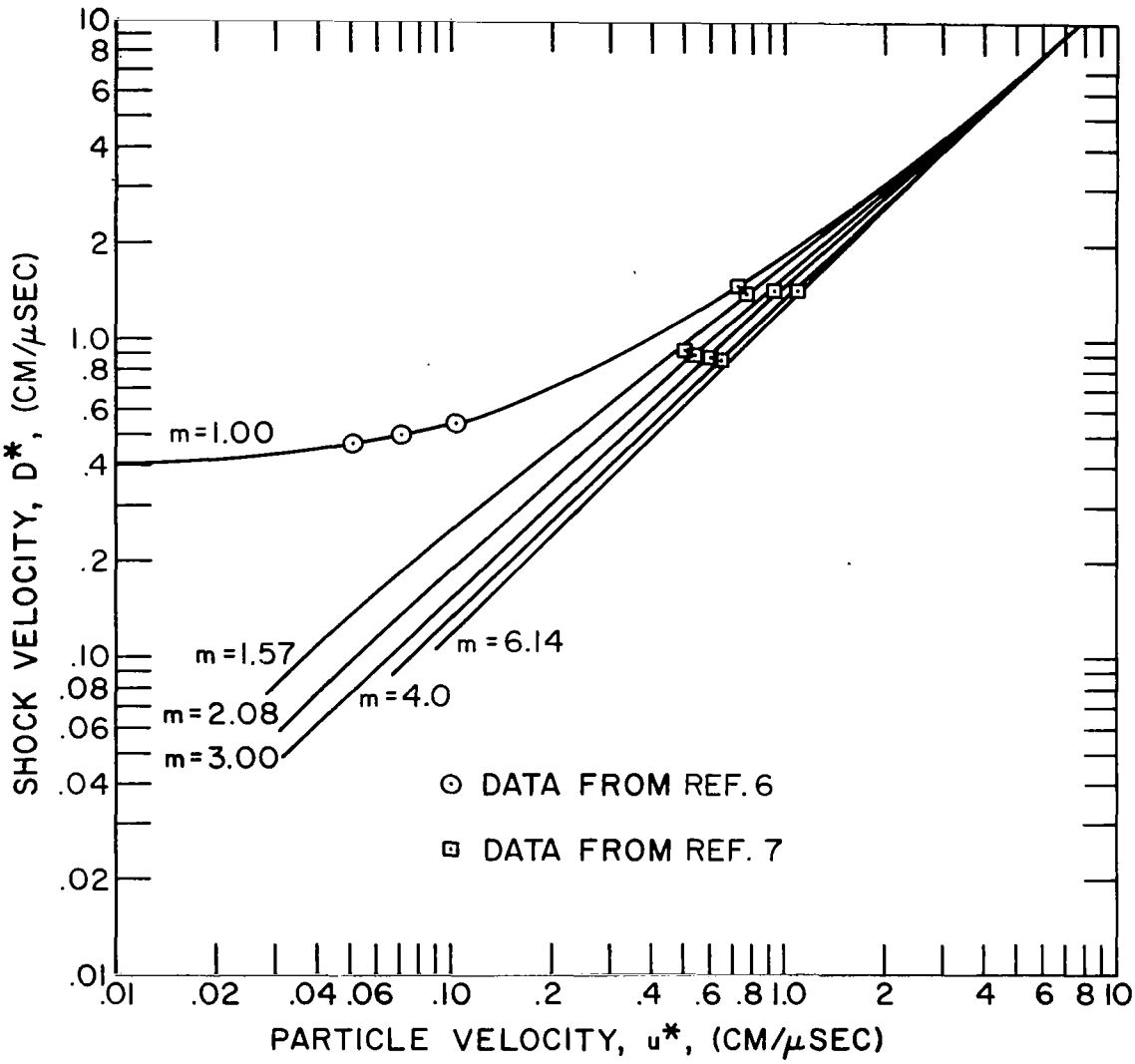

Figure 5. Hugoniots for Porous Copper - Modified Plate-Gap Model
(a) Shock Velocity vs Particle Velocity

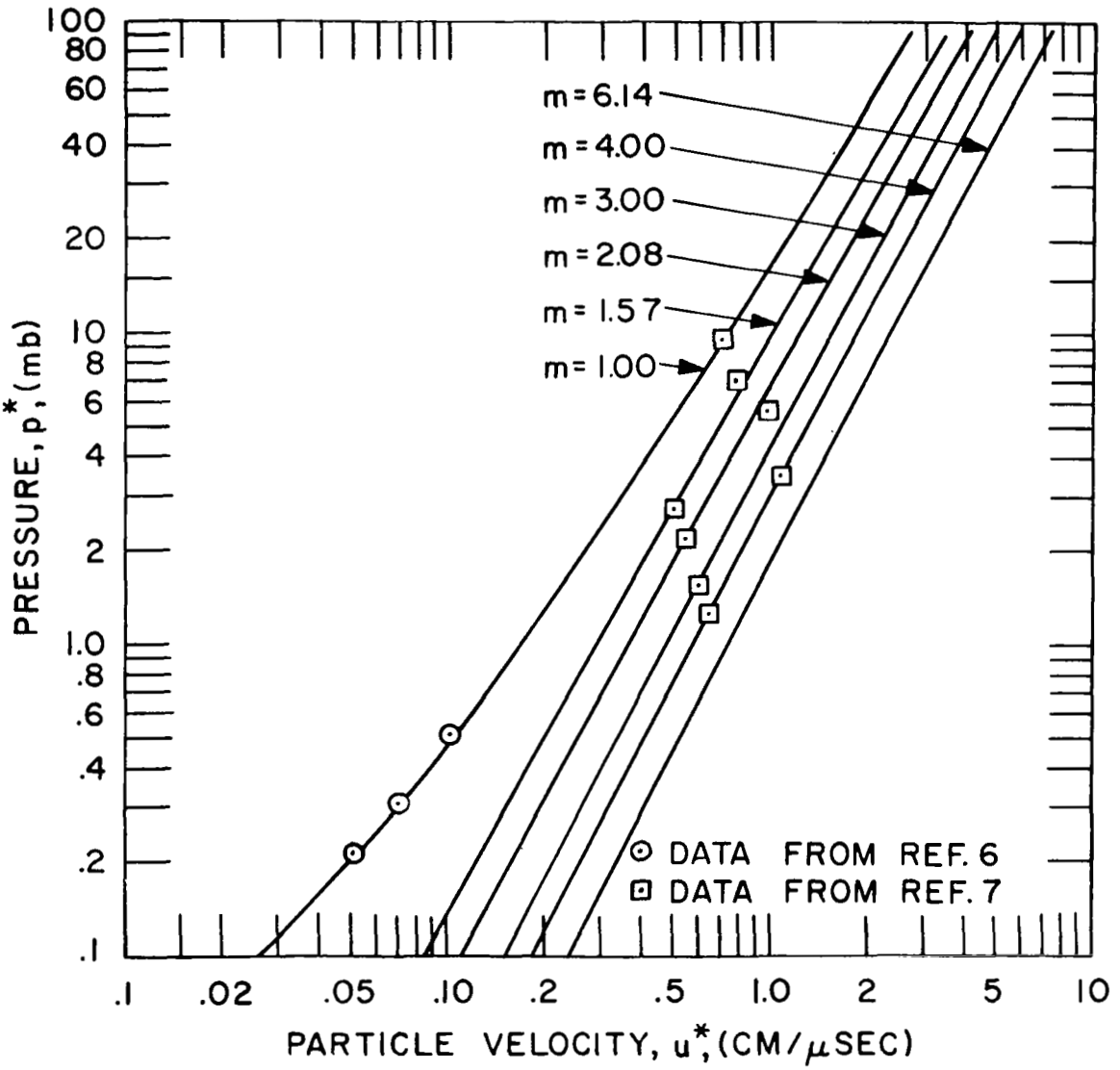

Figure 5. Hugoniots for Porous Copper - Modified Plate-Gap Model
(b) Pressure vs Particle Velocity

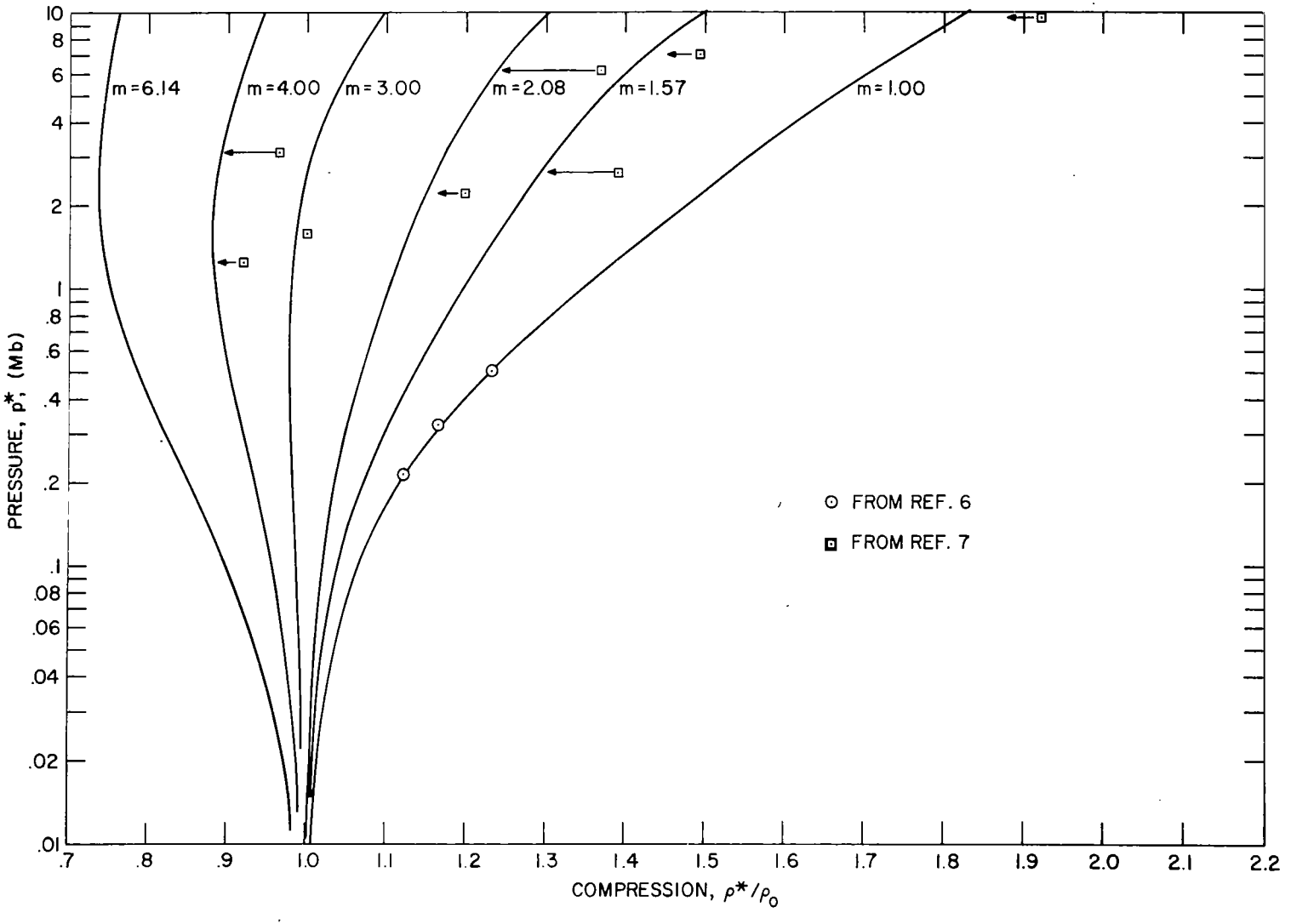

Figure 5. Hugoniots for Porous Copper - Modified Plate-Gap Model
(c) Pressure vs Compression

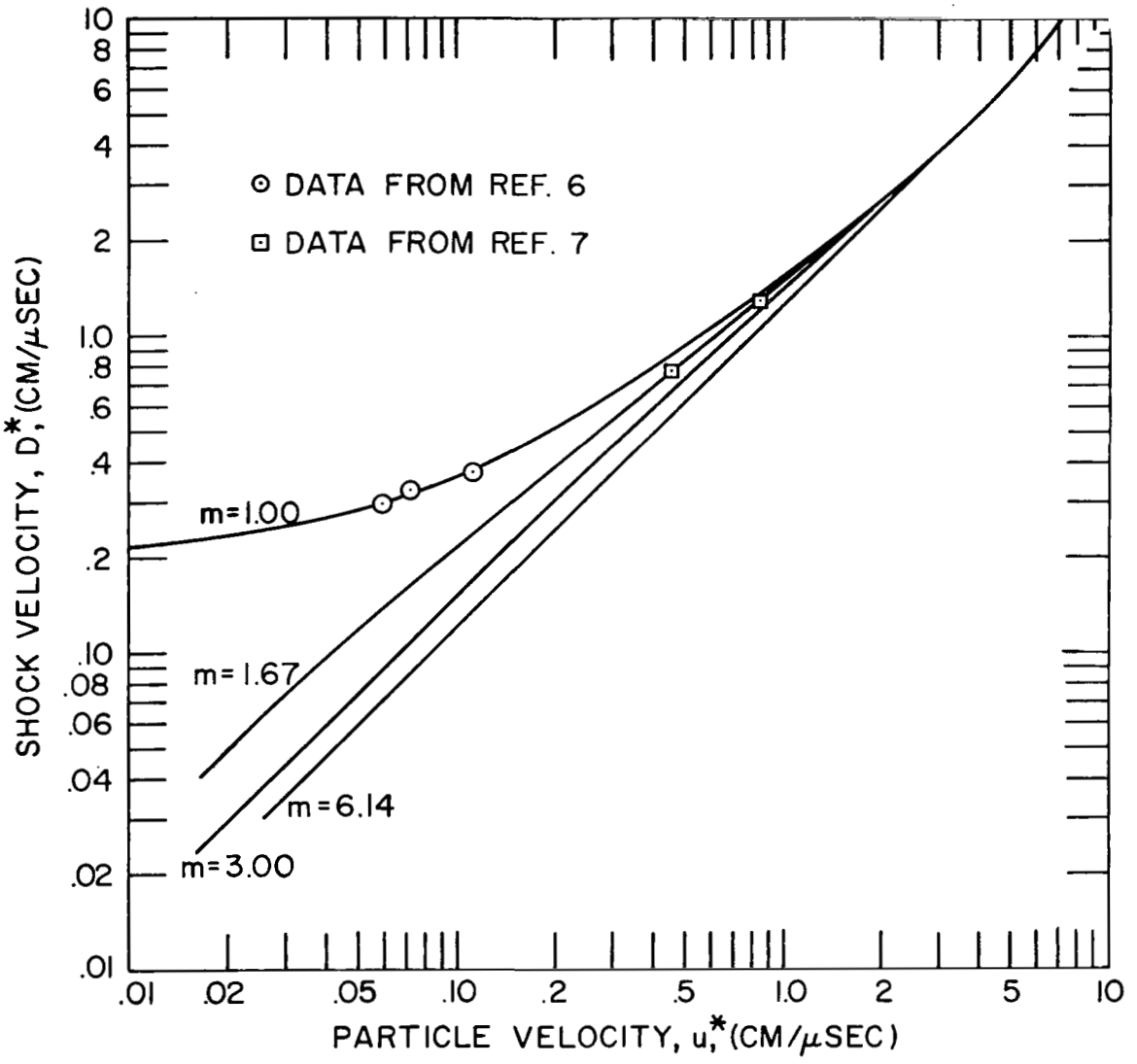

Figure 6. Hugoniots for Porous Lead - Modified Plate-Gap Model
(a) Shock Velocity vs Particle Velocity

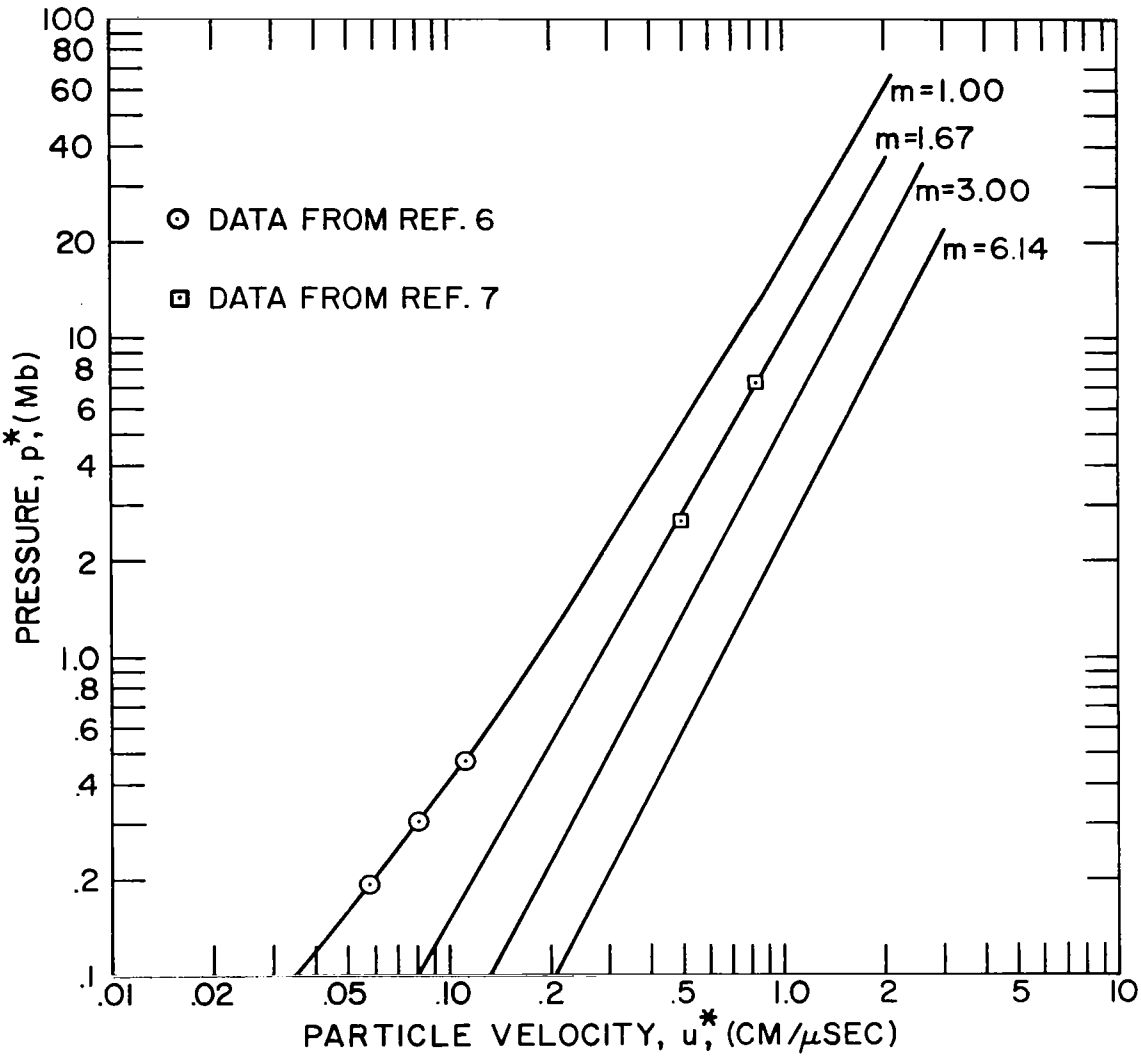

Figure 6. Hugoniots for Porous Lead - Modified Plate-Gap Model
(b) Pressure vs Particle Velocity

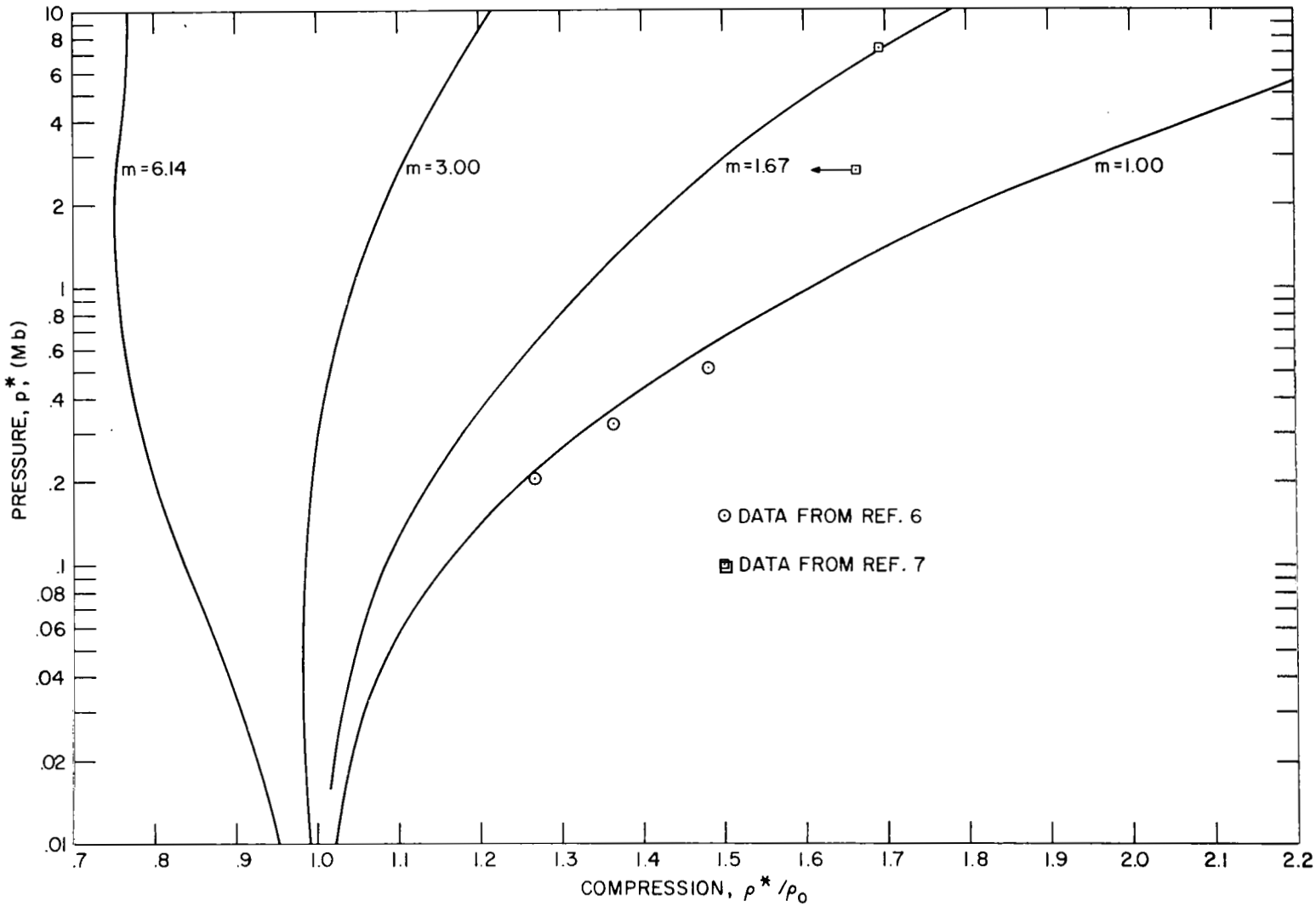

Figure 6. Hugoniots for Porous Lead - Modified Plate-Gap Model
(c) Pressure vs Compression

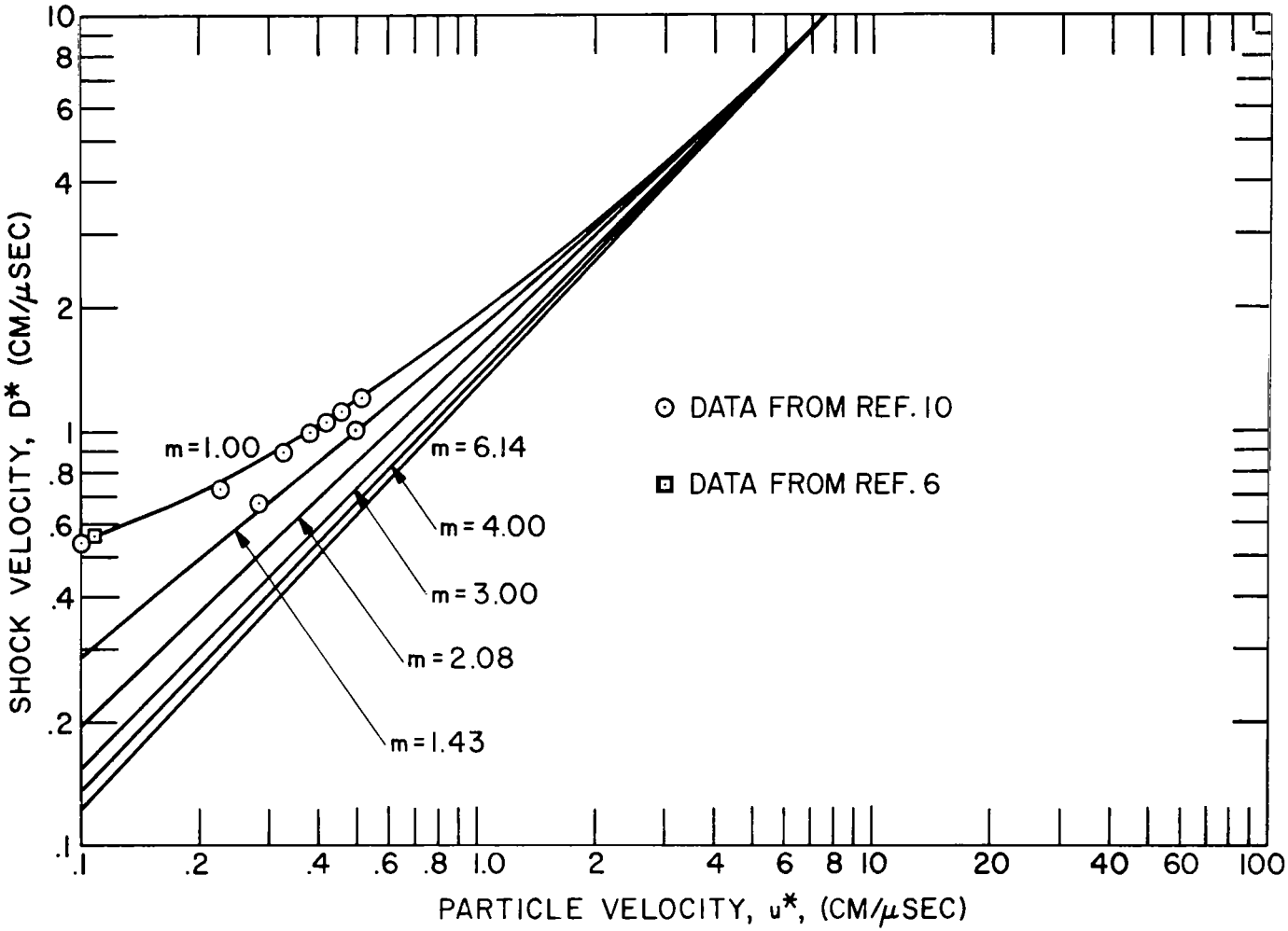

Figure 7. Hugoniots for Porous Iron - Modified Plate-Gap Model
(a) Shock Velocity vs Particle Velocity

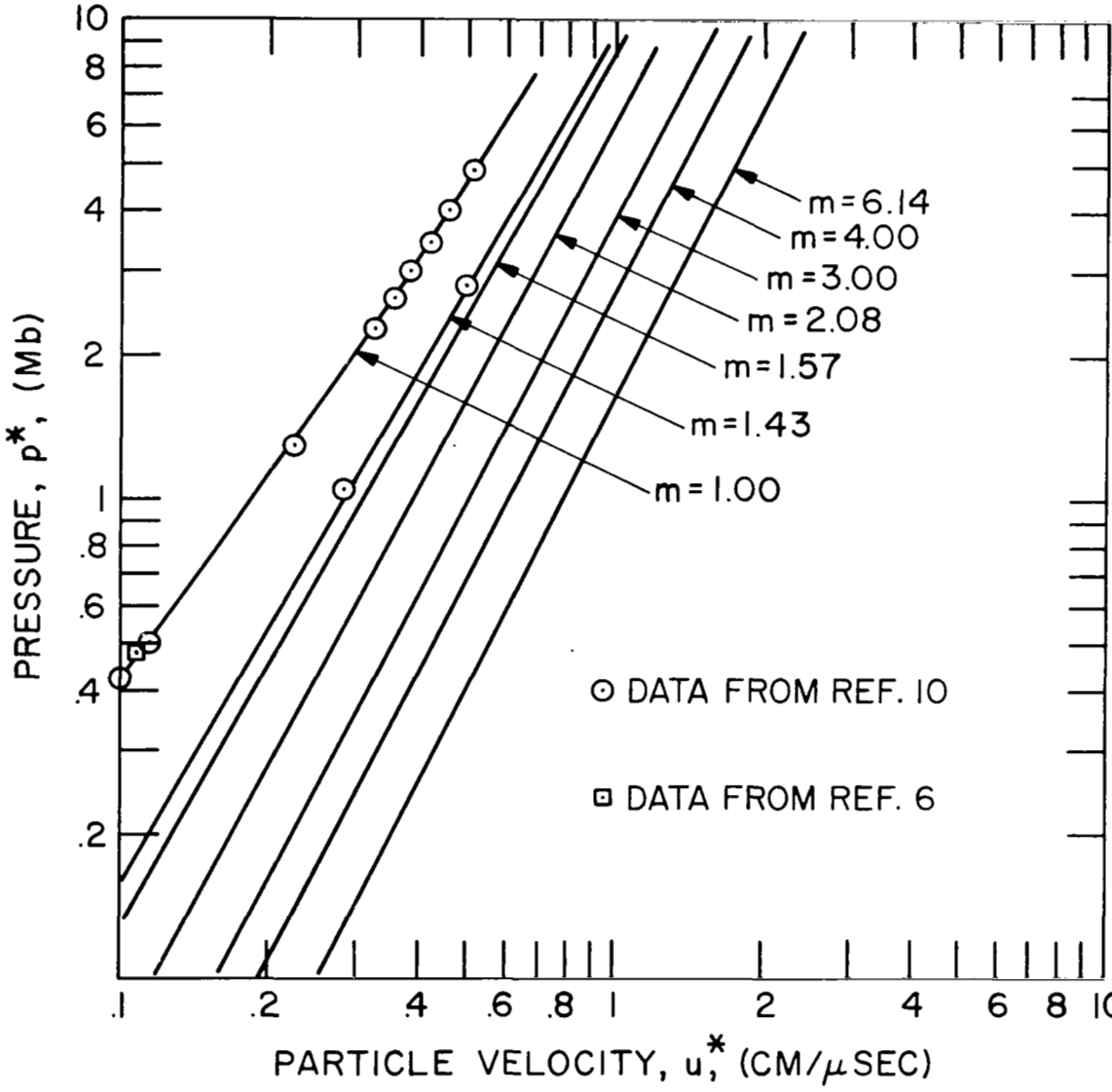

Figure 7. Hugoniots for Porous Iron - Modified Plate-Gap Model
(b) Pressure vs Particle Velocity

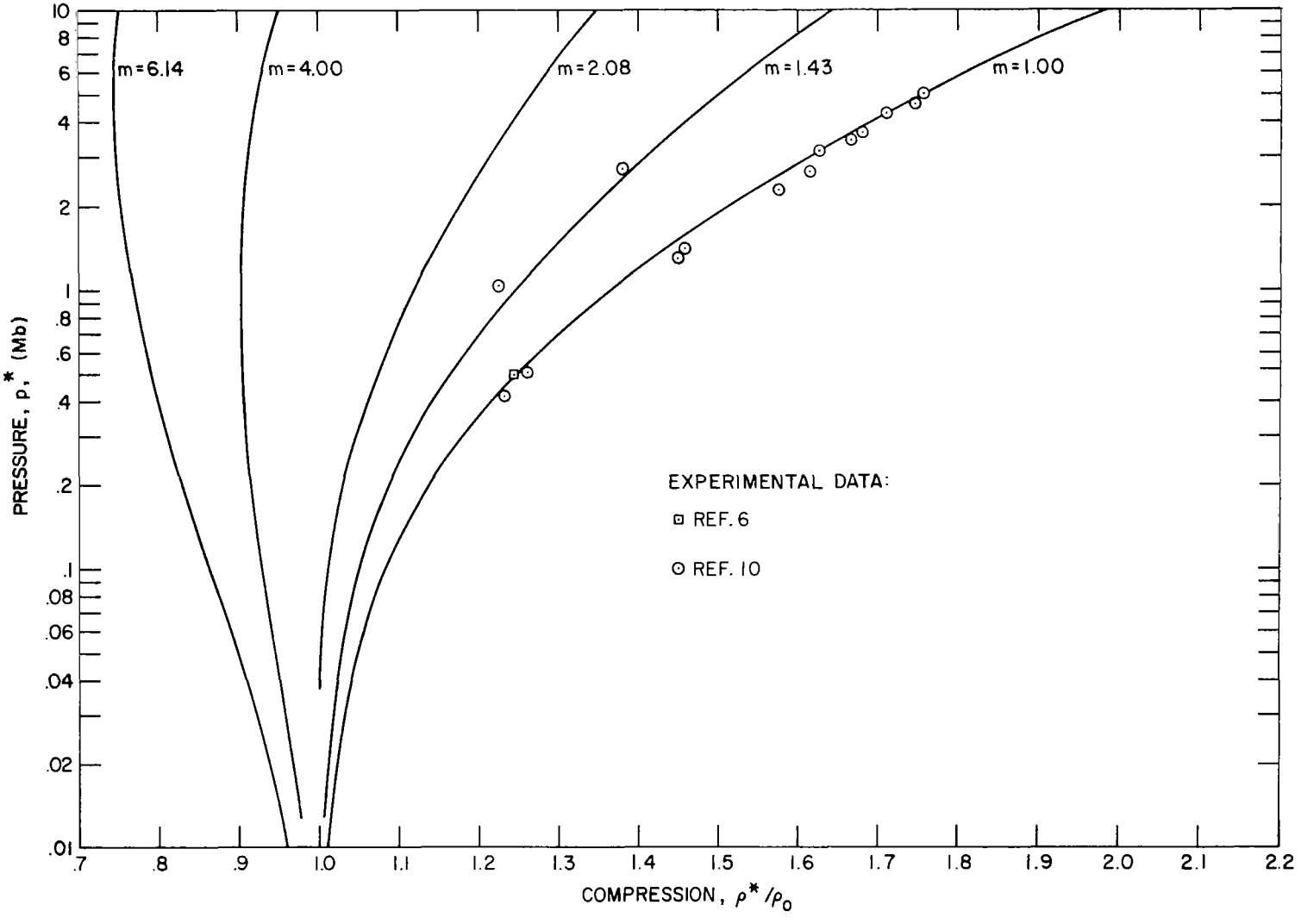

Figure 7. Hugoniots for Porous Iron - Modified Plate-Gap Model
(c) Pressure vs Compression

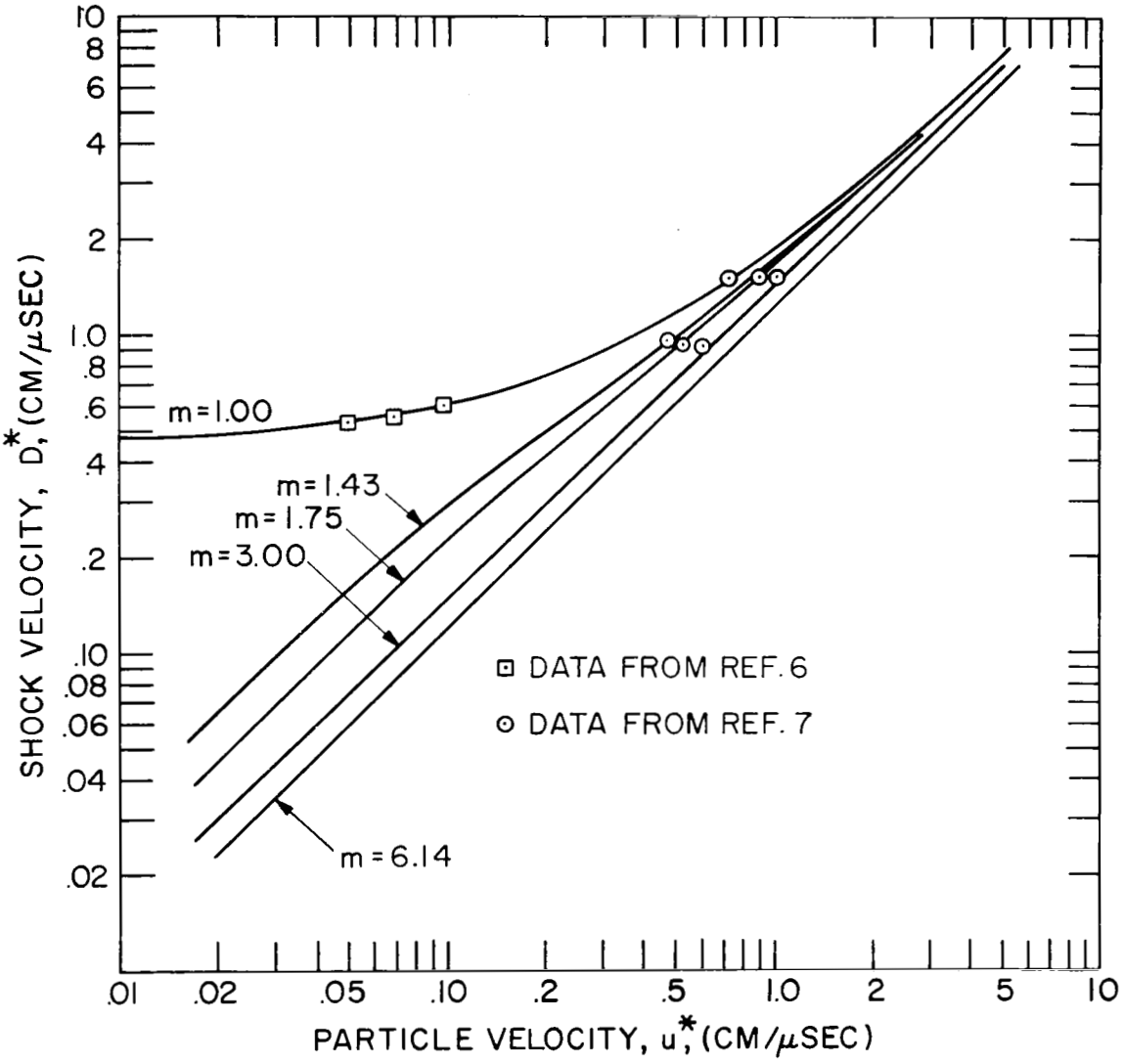

Figure 8. Hugoniots for Porous Nickel - Modified Plate-Gap Model
(a) Shock-Velocity vs Particle Velocity

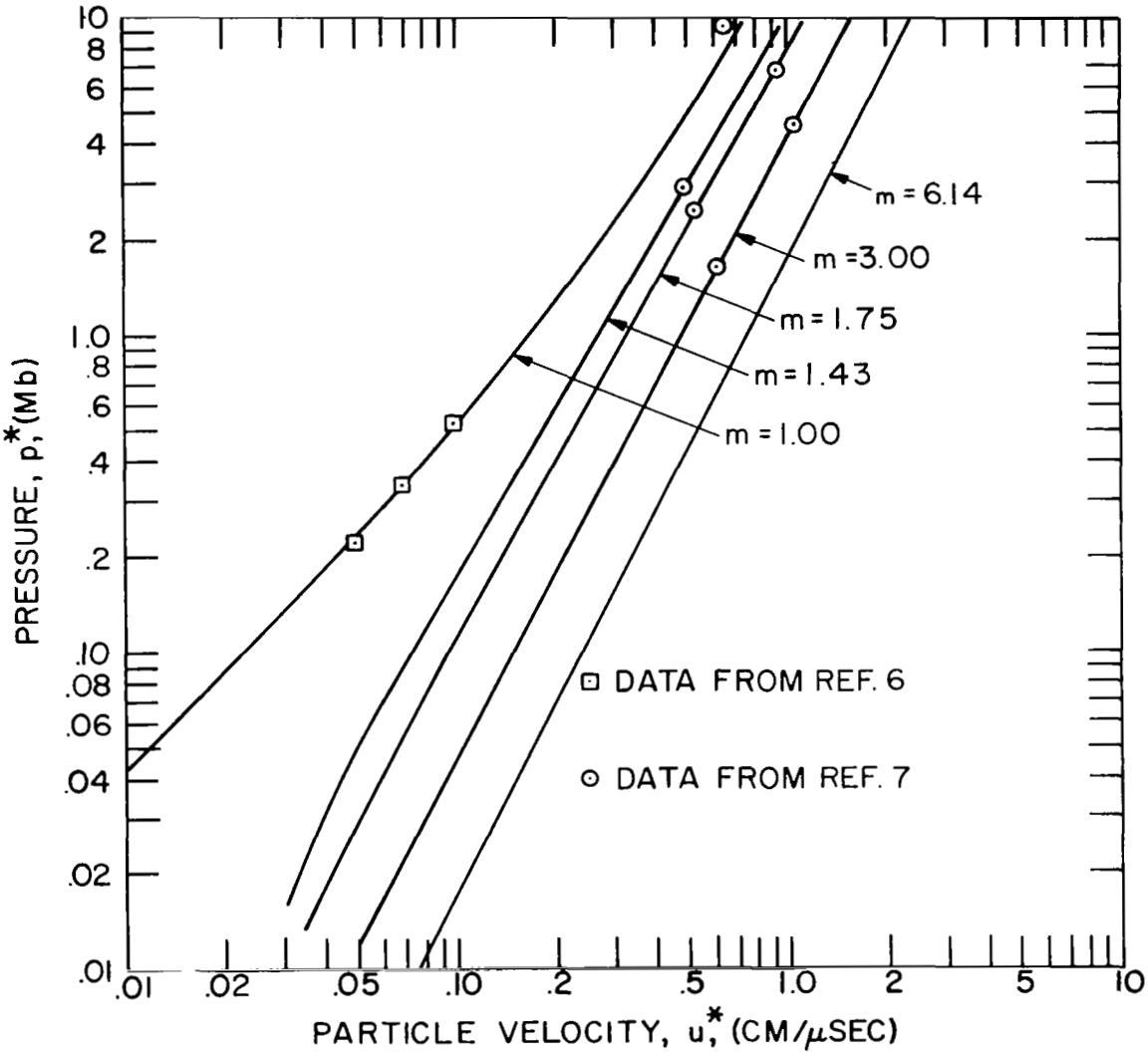

Figure 8. Hugoniots for Porous Nickel - Modified Plate-Gap Model
(b) Pressure vs Particle Velocity

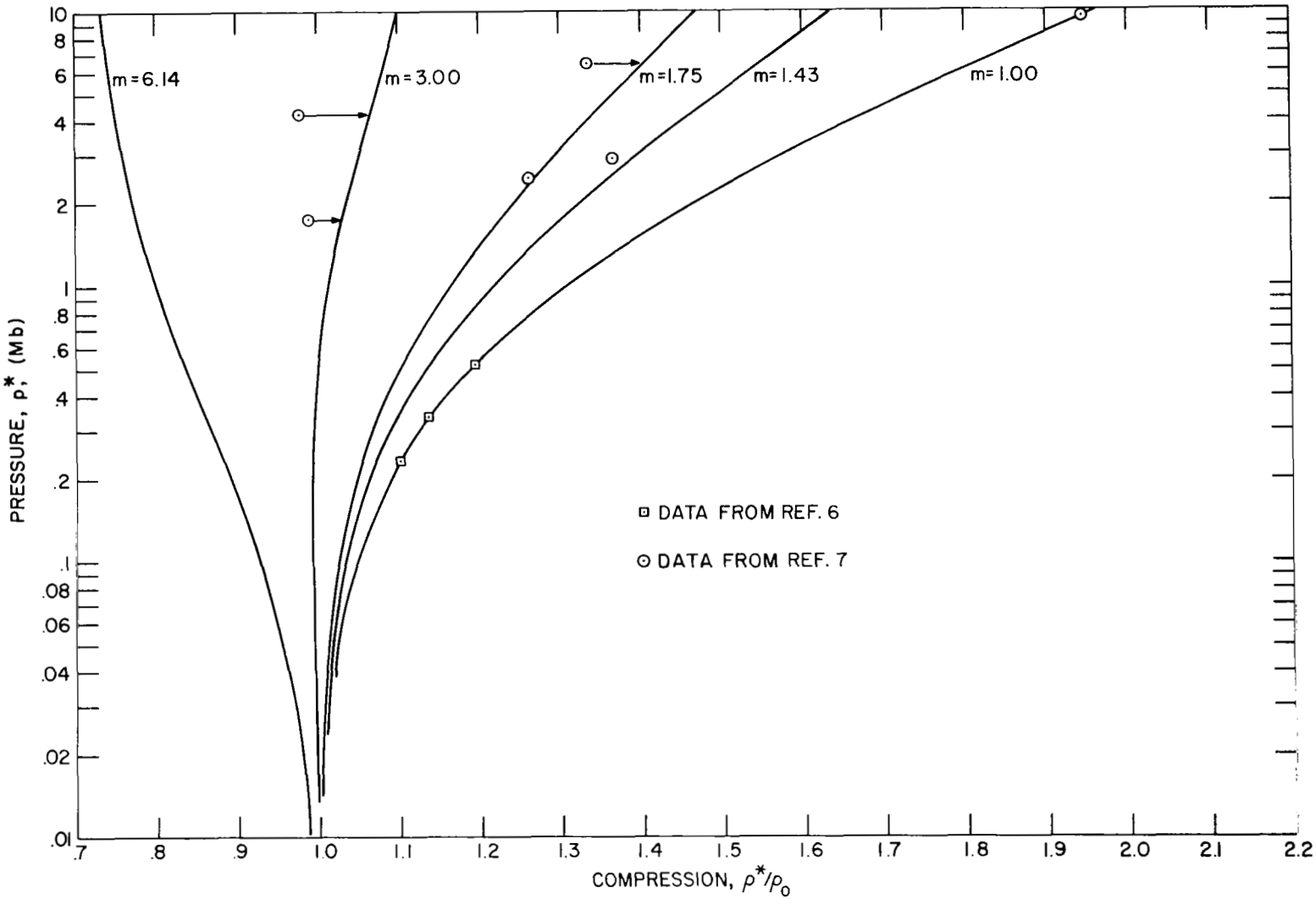

Figure 8. Hugoniots for Porous Nickel - Modified Plate-Gap Model
(c) Pressure vs Compression

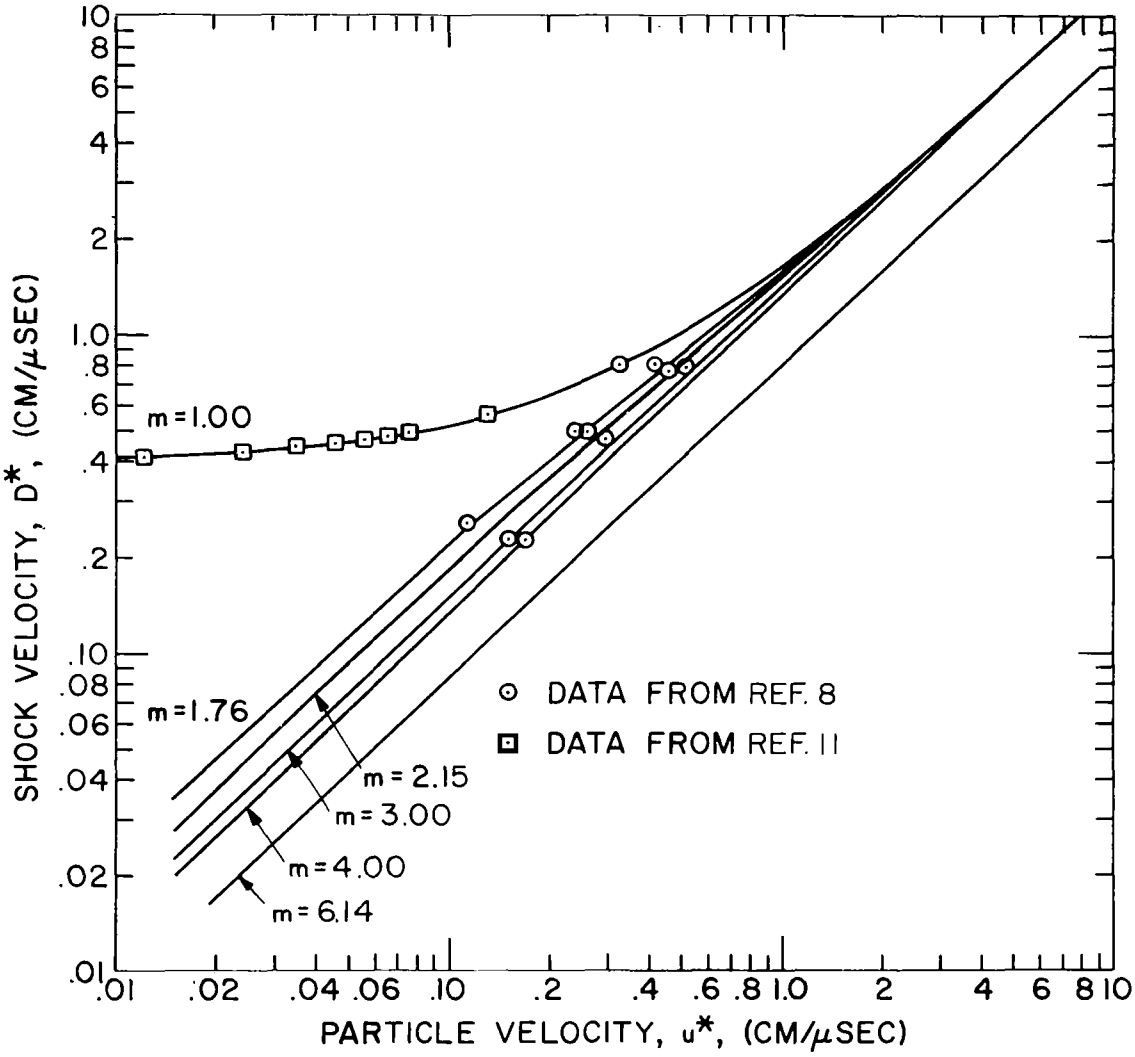

Figure 9. Hugoniots for Porous Tungsten - Modified Plate-Gap Model
(a) Shock Velocity vs Particle Velocity

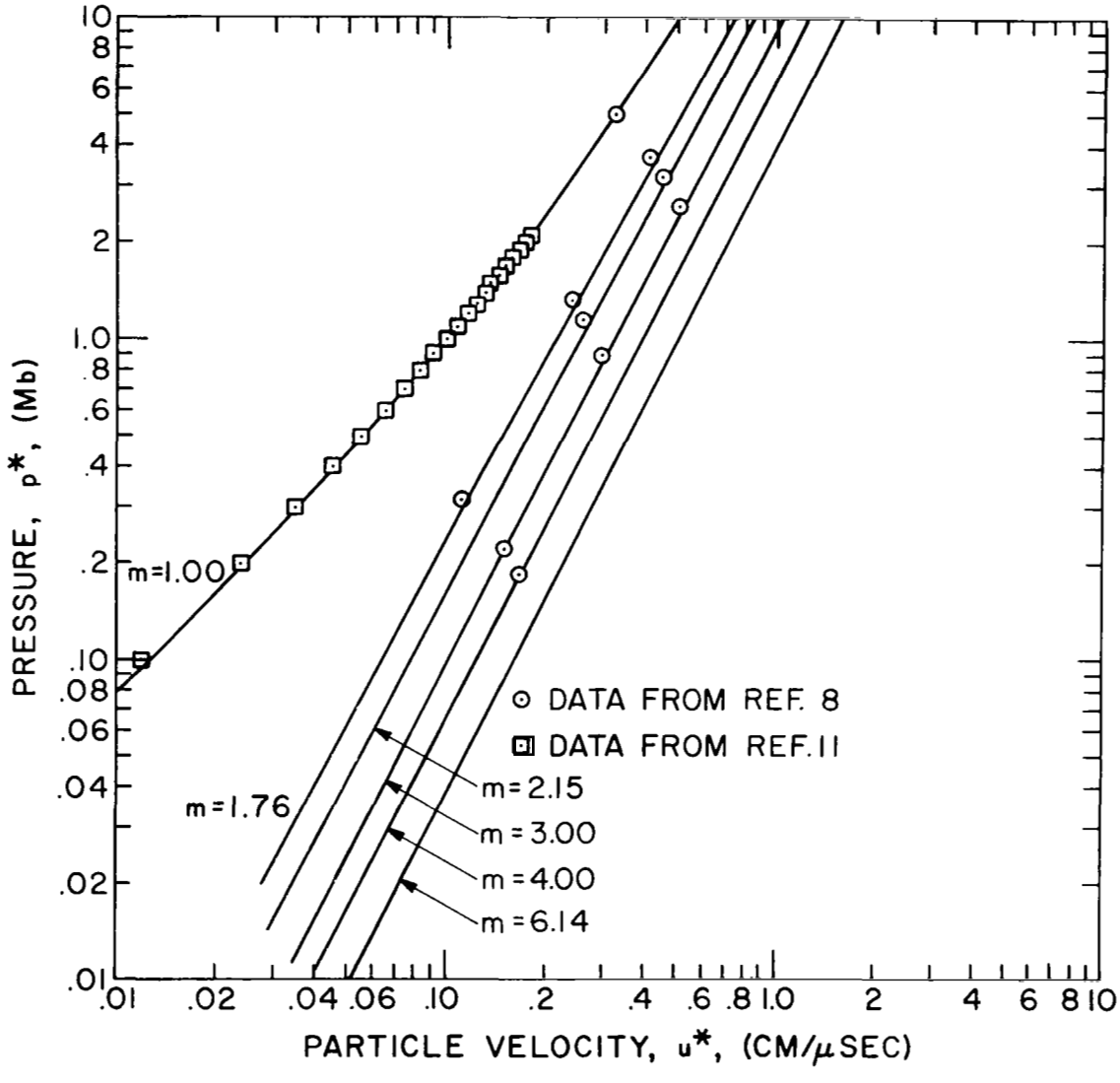

Figure 9. Hugoniots for Porous Tungsten - Modified Plate-Gap Model
(b) Pressure vs Particle Velocity

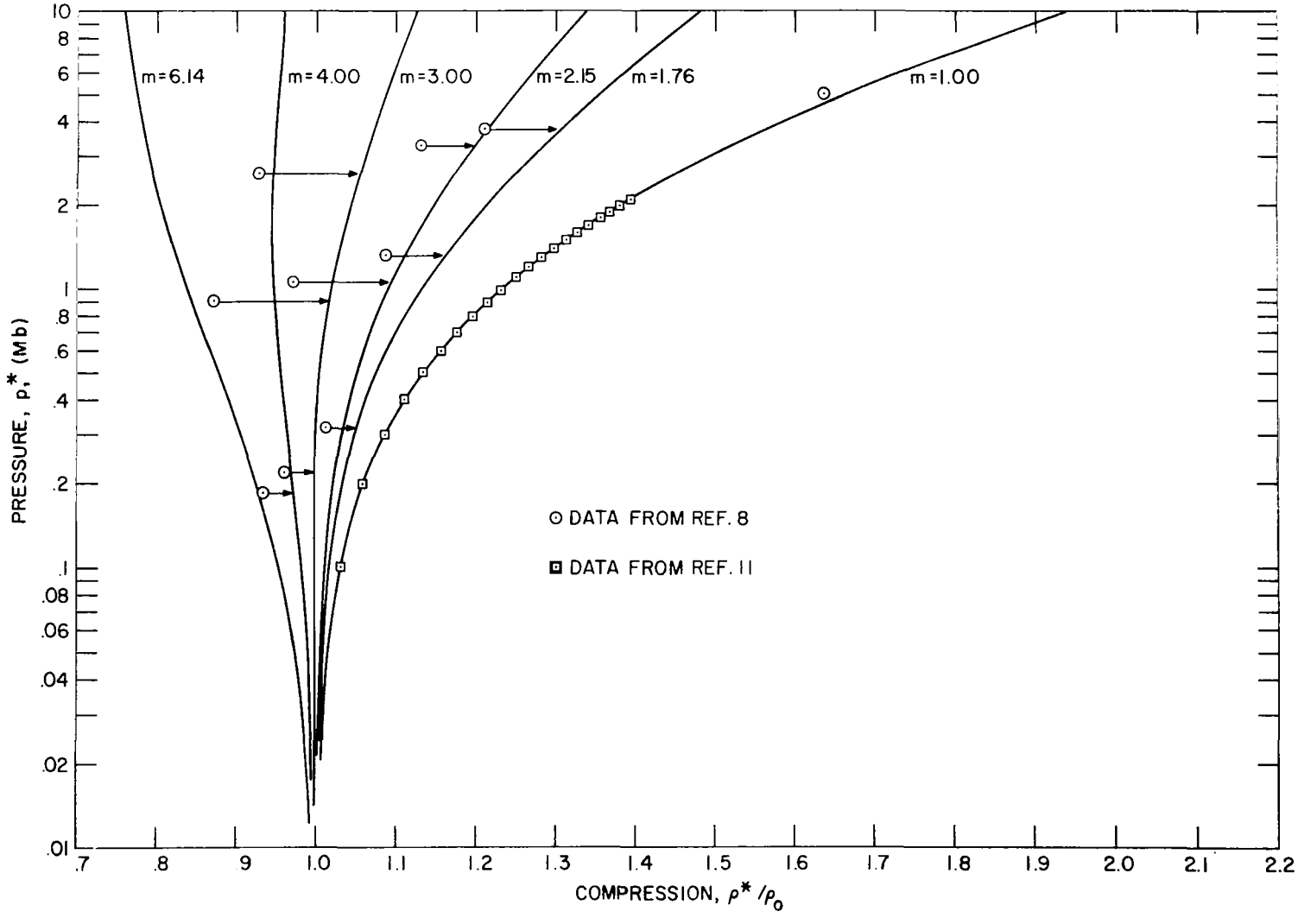

Figure 9. Hugoniots for Porous Tungsten - Modified Plate-Gap Model
(c) Pressure vs Compression

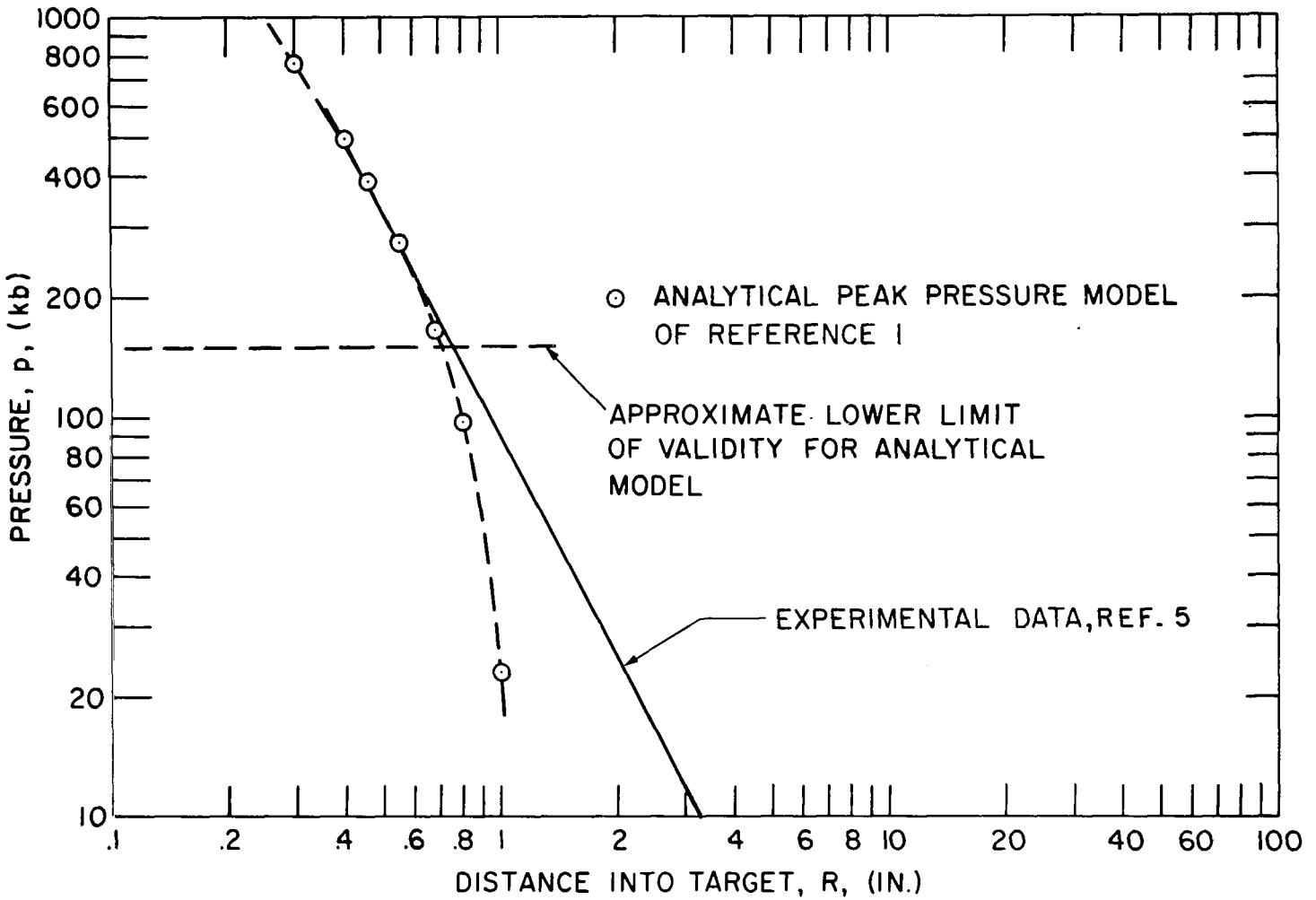

Figure 10. Peak Pressure in Aluminum Target Impacted by Cylindrical Aluminum Pellet of Mass 0.585 gm and $\ell/2L = 3.3$ at 11.15 Km/sec.

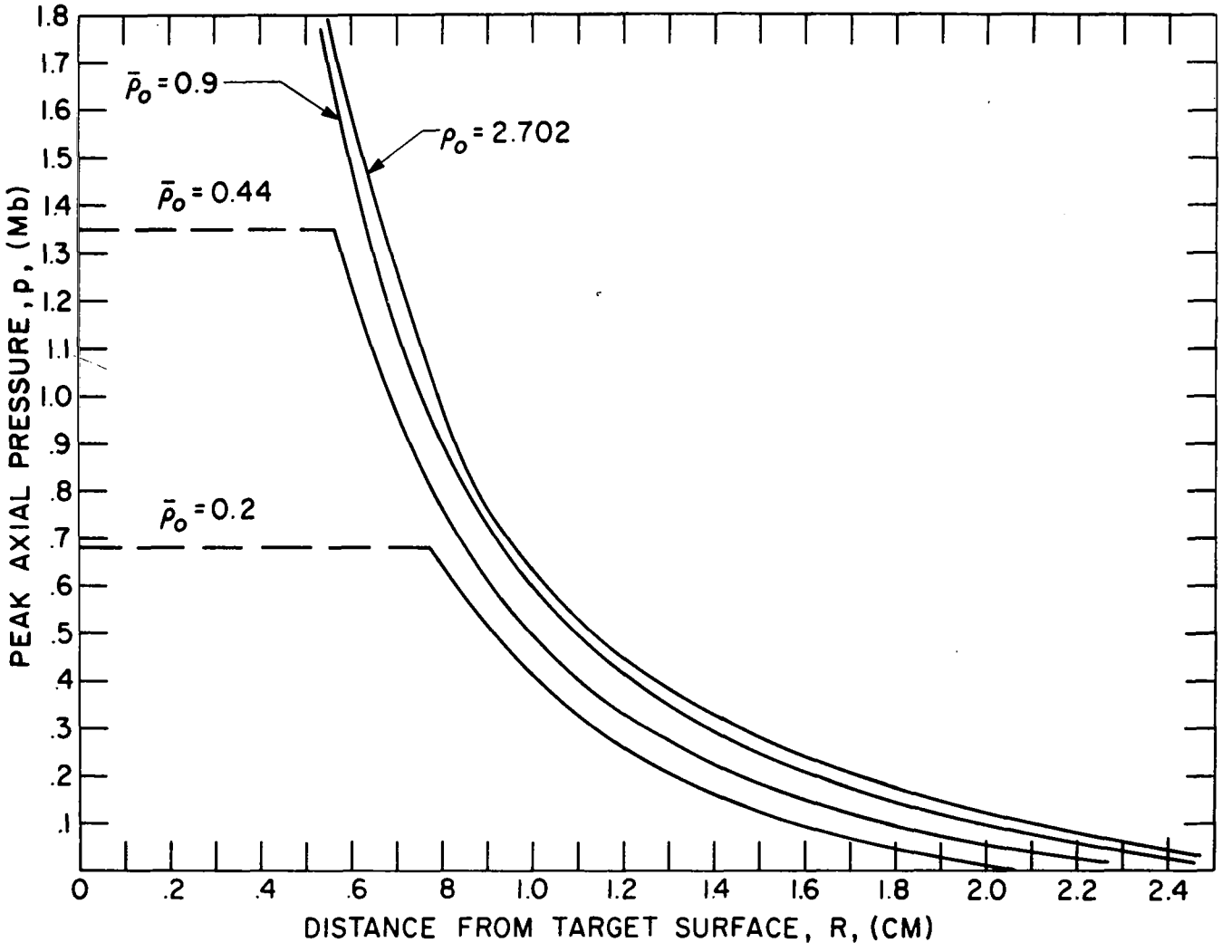

Figure 11. Calculated Peak Axial Pressure Based on Modified Plate-Gap Model Hugoniot - Solid Aluminum Target and Reduced Density Equi-Energy Aluminum Projectiles. Impact at 20 km/sec.

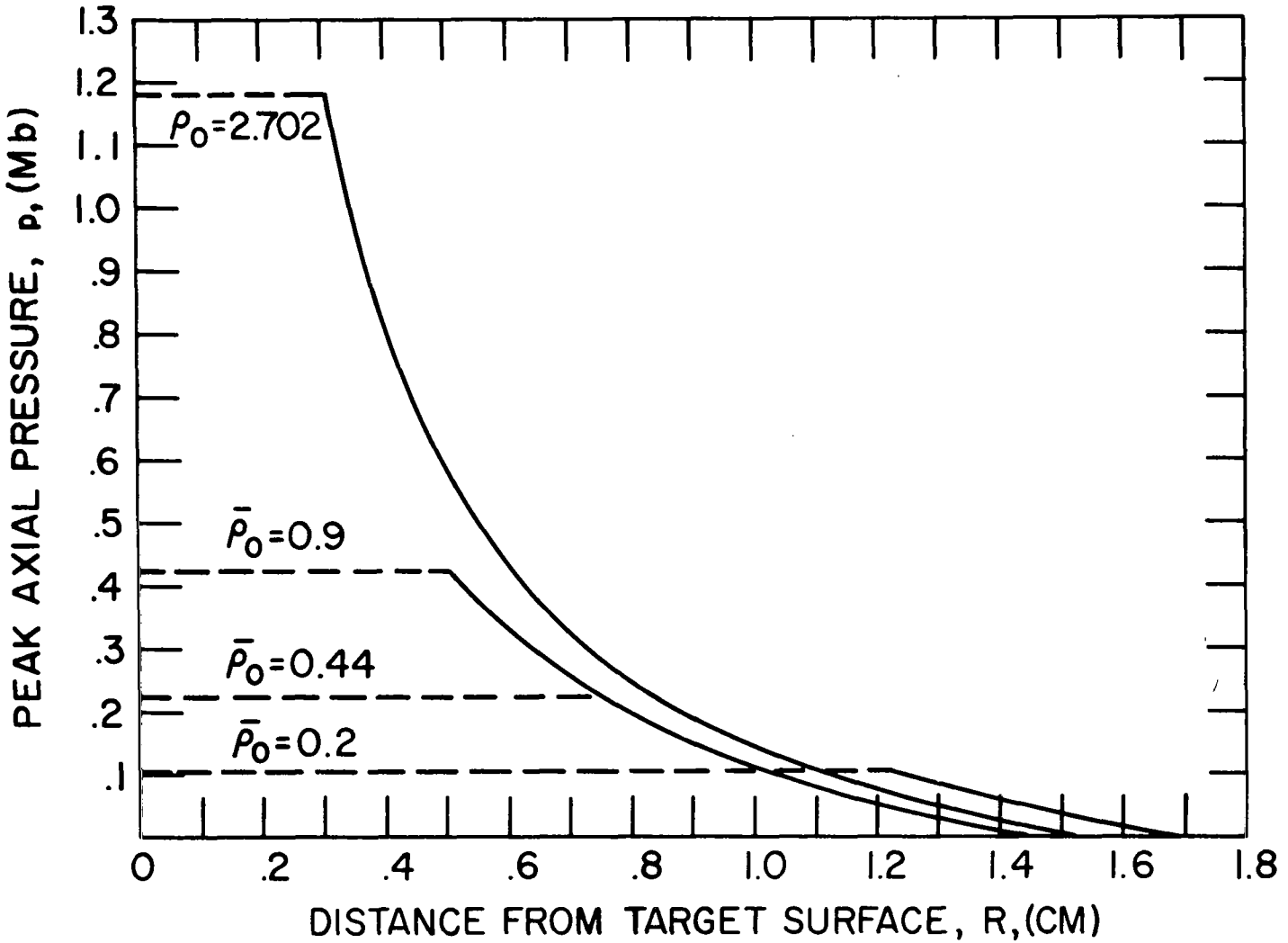

Figure 12. Calculated Peak Axial Pressure Based on Modified Plate-Gap Model Hugoniot - Solid Aluminum Target and Reduced Density Equi-Energy Aluminum Projectiles. Impact at 7.6 km/sec.

NATIONAL AERONAUTICS AND SPACE ADMINISTRATION
WASHINGTON, D. C. 20546

OFFICIAL BUSINESS

FIRST CLASS MAIL

POSTAGE AND FEES PAID
NATIONAL AERONAUTICS AND
SPACE ADMINISTRATION

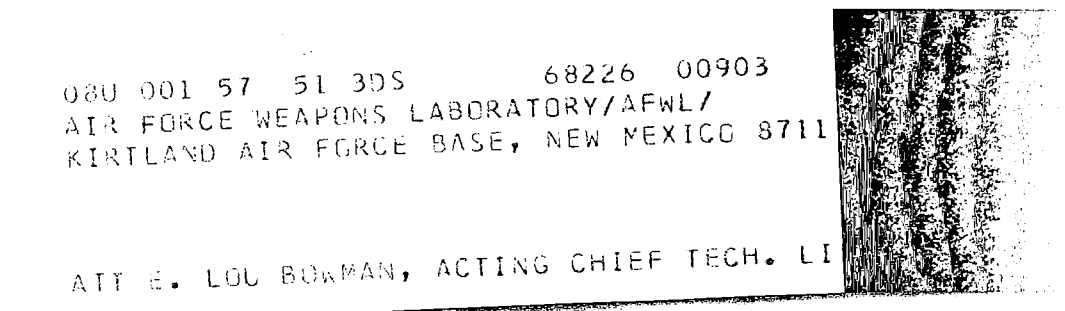

POSTMASTER: If Undeliverable (Section 158 Postal Manual) Do Not Return

"The aeronautical and space activities of the United States shall be conducted so as to contribute . . . to the expansion of human knowledge of phenomena in the atmosphere and space. The Administration shall provide for the widest practicable and appropriate dissemination of information concerning its activities and the results thereof."

—NATIONAL AERONAUTICS AND SPACE ACT OF 1958

NASA SCIENTIFIC AND TECHNICAL PUBLICATIONS

TECHNICAL REPORTS: Scientific and technical information considered important, complete, and a lasting contribution to existing knowledge.

TECHNICAL NOTES: Information less broad in scope but nevertheless of importance as a contribution to existing knowledge.

TECHNICAL MEMORANDUMS: Information receiving limited distribution because of preliminary data, security classification, or other reasons.

CONTRACTOR REPORTS: Scientific and technical information generated under a NASA contract or grant and considered an important contribution to existing knowledge.

TECHNICAL TRANSLATIONS: Information published in a foreign language considered to merit NASA distribution in English.

SPECIAL PUBLICATIONS: Information derived from or of value to NASA activities. Publications include conference proceedings, monographs, data compilations, handbooks, sourcebooks, and special bibliographies.

TECHNOLOGY UTILIZATION PUBLICATIONS: Information on technology used by NASA that may be of particular interest in commercial and other non-aerospace applications. Publications include Tech Briefs, Technology Utilization Reports and Notes, and Technology Surveys.

Details on the availability of these publications may be obtained from:

SCIENTIFIC AND TECHNICAL INFORMATION DIVISION

NATIONAL AERONAUTICS AND SPACE ADMINISTRATION

Washington, D.C. 20546